Fabrication of Nanoscale Josephson Junctions and Superconducting Quantum Interference Devices

by

Feyruz Kitapli

A thesis
presented to the University of Waterloo
in fulfillment of the
thesis requirement for the degree of
Master of Applied Science
in
Mechanical Engineering - Nanotechnology

Waterloo, Ontario, Canada, 2011

AUTHOR'S DECLARATION

I hereby declare that I am the sole author of this thesis. This is a true copy of the thesis, including any required final revisions, as accepted by my examiners.

I understand that my thesis may be made electronically available to the public.

Abstract

Fabrication of nanoscale Josephson junctions and Superconducting Quantum Interference Devices (SQUID) is very promising but challenging topic in the superconducting electronics and device technology. In order to achieve best sensitivity of SQUIDs and to reproduce them easily with a straightforward method, new fabrication techniques for realization of nanoSQUIDs needs to be investigated.

This study concentrates on investigation of new fabrication methodology for manufacturing nanoSQUIDs with High Temperature Bi-Crystal Grain Boundary Josephson Junctions fabricated onto SrTiO3 bi-crystal substrates using YBa2Cu3O7-δ (YBCO) thin-films.

In this process nanoscale patterning of YBCO was realized by using electron beam patterning and physical dry etching of YBCO thin films on STO substrates. YBCO thin films were deposited using RF magnetron sputtering technique in the mixture of Ar and O_2 gases and followed by annealing at high temperatures in O_2 atmosphere. Structural characterization of YBCO thin films was done by Scanning Electron Microscope (SEM) and Energy Dispersive X-ray Spectroscopy (EDX). Superconducting properties of thin films was characterized by AC magnetic susceptibility measurements. Nanoscale structures on YBCO thin films were fabricated by one E-Beam Lithography (EBL) step followed by Reactive Ion Etching (RIE) and physical dry etching. First SiO_2 thin film were deposited on YBCO by RF magnetron sputtering and it was patterned by EBL using Polystyrene (PS) as resist material and RIE. Then SiO_2 was used as an etch mask for physical dry etching of YBCO and nanoscale structures on YBCO were formed.

Acknowledgements

It is my pleasure to express my sincere gratitude to my supervisor Prof. Mustafa Yavuz for his support throughout this study.

I have been lucky to have had the chance to meet and work with Prof. Bo Cui. I am deeply indebted to him for instructing me in the appropriate attitudes towards research as well as his guidance, support and encouragement.

I would like to express my sincere thanks to Dr. Ahmet Kilic for sharing his experience and friendship.

I am thankful to my friends in the University of Waterloo for their friendship and support.

Finally, I would like to express my gratitude and love to my family who has always supported and encouraged me.

Table of Contents

List of Figures

Chapter 1

Introduction

Josephson junctions are the main building blocks of superconducting electronic devices and there was a huge progress in development of high temperature superconducting (HTS) Josephson junction technology at last decades after discovery of high temperature superconductivity. They are utilized in SQUIDs, terahertz devices, rapid single flux quantum (RSFQ) logic circuits and they are also promising element for future quantum computers. But fabrication of nanoscale Josephson junctions with a straightforward, scalable and reproducible method is current challenge in high temperature superconducting electronics technology.

A Josephson junction is defined by two superconductors separated by a thin insulating barrier. Cooper pairs can tunnel through the barrier, forming a current with no voltage dissipation across the junction. Josephson junctions which have been fabricated using conventional low-temperature superconductors are usually in superconductor/insulator/superconductor configuration. But for high temperature superconducting junctions, many structures have been investigated to fabricate reproducible and stable junctions. Since the discovery of Josephson Effect on the natural grain-boundaries of high temperature superconductors, there was a huge effort to fabricate Josephson junctions and SQUIDs with variety of device structures. Bicrystal grain boundary, step-edge grain boundary, step-edge superconductor/normal-metal/superconductor (SNS), ramp-edge SNS, ion beam damaged and interface-engineered junctions are the most popular configurations.[1] This progress in HTS Josephson junction technology is mostly driven by expectations that wide usage of superconductors is possible which is cooled in liquid nitrogen at 77 K than liquid helium at 4.2 K. Because, liquid nitrogen is much cheaper than liquid helium and it is more stable. But HTS Junction

fabrication technology is not standardized as its low temperature counterpart. There are many methods and materials for fabrication of HTS Josephson junctions. But grain boundary junctions formed on YBCO during epitaxial growth on bicrystal substrates is one of the most suitable methods for fabrication of high temperature superconductor devices. YBCO is popular among high temperature superconductors because of its convenient crystal structures for variety of applications, high critical current density and relatively low level of *1/f* noise.[2] And grain boundary junctions of YBCO offers stability and reproducibility for Josephson devices.

Recently YBCO nanoSQUIDs were fabricated by using Focused Ion Beam Technology and it offers very low noise levels and high spin sensitivity. In order to improve noise characteristics and spin sensitivity further miniaturization of devices is required. [3] Fabrication of YBCO nanowires as narrow as 10 nm in width was realized and their superconducting properties are characterized to be useful for superconducting electronic devices. These recent progresses encourage us to investigate new fabrication methods for nanoSQUIDs. Fabrication of NanoSQUIDs which would be capable of detecting small spin number of magnetic particles directly coupled to SQUID loop seems possible in near future.

This thesis is dedicated to investigation of new fabrication methods for nanoSQUIDs by using Electron Beam Lithography. In Chapter 2 general information about superconductivity was given. Chapter 3 gives detailed information about theory of Josephson junctions and SQUIDs. Different fabrication methods for Josephson junctions were discussed in Chapter 4. Fabrication procedure for realization of Josephson junctions and nanoSQUIDs by using Electron Beam Lithography was investigated in Chapter 5. Main results on studied procedure were discussed and the thesis was concluded in Chapter 6.

Chapter 2

Superconductivity

2.1 History of Superconductivity

In 1908 Heike Kammerlingh Onnes succeeded in liquefying helium. And he was capable to investigate the electrical resistance of metals at very low temperatures. Mercury was among the purest of metals that Onnes obtained. Experiments on mercury were as predicted in the beginning. The resistance decreased with temperature.But when temperature reached 4.2 K, the resistance suddenly dropped to zero. This was thought to be because of short circuit in the system, but different experiments with different configurations resulted same. Resistance reappeared when temperature is rised. Similar experiments were performed on lead and tin, which showed the same results at 7.2 K and 3.7 K respectively. These temperatures were named as critical temperatures, and the effect was named superconductivity. Onnes received the Nobel Prize in 1913 for the discovery of superconductivity and the liquefaction of helium. Onnes discovered another effect while he was trying to find uses for superconductors. Magnetic fields above certain field strength destroyed the superconductivity. This value is named as critical magnetic field (Hc), and it is different for each material. [5]

In 1933 W. Meissner and R. Oschenfield observed that superconductors expel any applied magnetic fields while in the superconducting state. This phenomenon was called the Meissner effect. In order to prove a material's superconductivity both zero resistance and Meissner effect must be observed when it is cooled below its critical temperature [6].

In 1935, Fritz and Heinz London attempted to formulate model of superconductivity, The formulation is called the London Theory [7]. Vitaly Ginzburg and Lev Landau extended this theory in 1950 and introduced the idea of an order parameter and the concept of a coherence length.

In 1957, Bardeen, Cooper and Schrieffer constructed a theory which includes all the known parameters of superconductivity. It is called BCS theory and they are rewarded Nobel Prize in 1972. In 1986, Alex Müller and George Bednorz discovered high-temperature superconductivity. They found that a lanthanum-barium-copper-oxide shows superconducting properties at 30 K [8]. And they earned the Nobel Prize in physics in 1987.

In 1987 Wu et al discovered that yttrium-barium-copper-oxide (YBCO) had transition temperature of 93 K. YBCO was the first material that shows critical temperature above boiling point of liquid nitrogen (77 K) and it is one of the most popular high temperature superconductors today.
And Researchers are still trying to discover superconductors with higher transition temperature for realization of room temperature superconductivity.

2.2 Basics of Superconductivity

As mentioned before there are two main properties of superconductors; perfect conductivity and perfect diamagnetism. Resistivity of normal metals decrease with decreasing temperature depending on scattering mechanism of electrons, phonons and defects in materials. But in case of superconductors, resistance abruptly drops to zero at certain temperatures which is called transition temperature. And perfect conductivity occurs at the temperatures below transition temperature. Detected resistance in this state is beyond the sensitivity of state of art testing equipment.

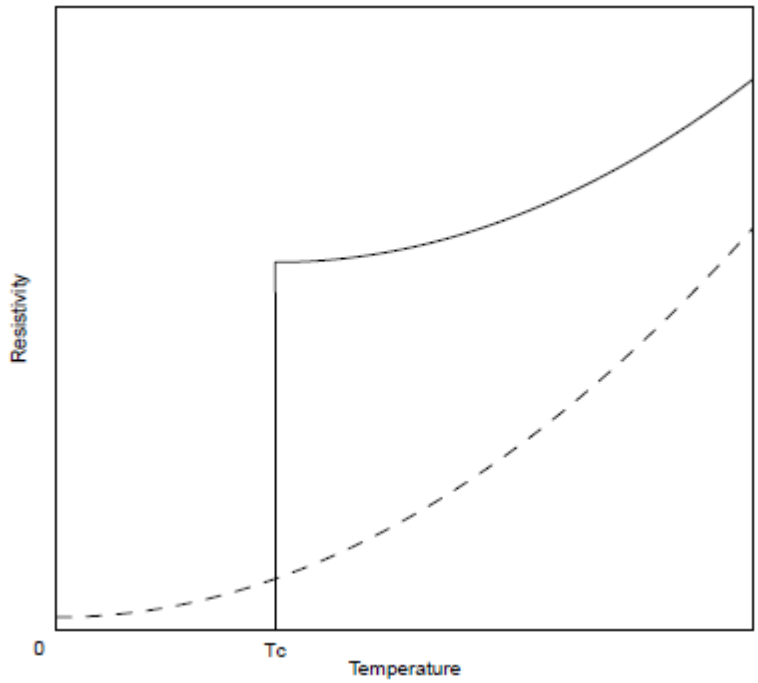

Figure 2.1: Temperature versus resistivity of a normal metal and of a superconductor [5].

Perfect conductivity can be demonstrated by applying external magnetic field to a superconducting ring and cooling it below transition temperature. If the magnetic field is removed, induced current around superconducting ring flow continuously and produce own magnetic flux. There will be no detectable decay in this magnetic flux in huge number of years.

And in this experiment, magnetic flux seen in the superconducting ring can only take values of integer multiplies of the value $2.067 \times 10^{15}\ Wb$ called magnetic flux quantum. Magnetic flux quantum is also equal to the Plank`s constant divided by charge of 2 electrons.

Low temperature is not the only condition superconductivity to be occurred. Magnetic fields higher than critical magnetic field of the material also can disturb the superconductivity. And critical

magnetic field is also depending on the temperature. The relationship between critical magnetic field temperature and transition temperature of superconductor is given by;

$$H_c(T) = H_c(0)[1 - (T/Tc)^2] \quad (2.1)$$

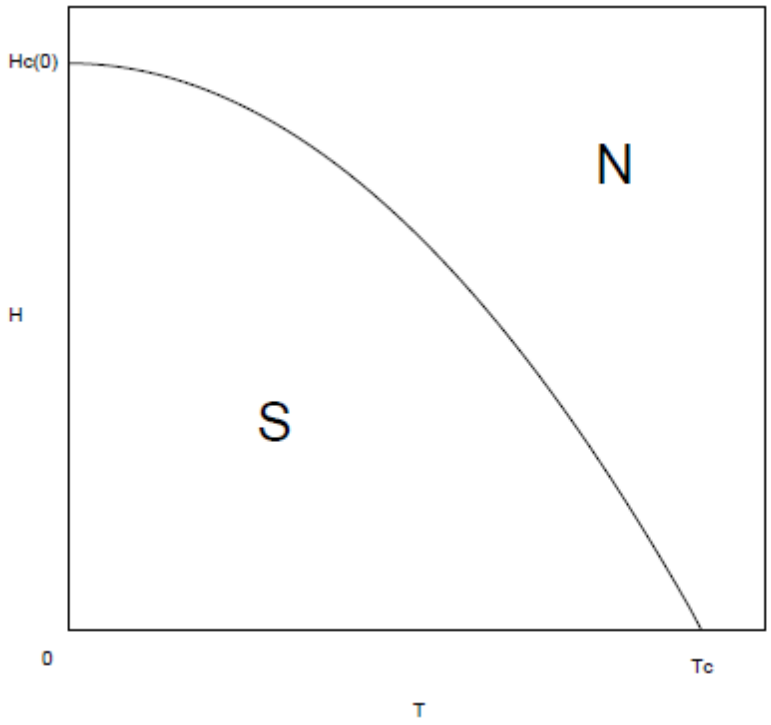

Figure 2.2: Temperature dependence of the critical magnetic field. The normal and superconductive state is above and below Hc(T) respectively.[5]

Superconductors are also perfect diamagnetic materials which distinguish them from ideal perfect conductors. In superconducting state these materials expel applied magnetic field by producing surface currents which induce opposing magnetic field. This was the phenomenon which is called as Meissner effect [9].

2.3 London Equations

The London equations are formulated to describe the superconductivity according to observed physical phenomena. Formulation starts with the Drude model for electrical conductivity. It can be written as

$$m\frac{d\mathbf{v}}{dt} = e\mathbf{E} - \frac{m\mathbf{v}}{\tau} \tag{2.2}$$

Where **v** is the average velocity of electrons and $\boldsymbol{\tau}$ is the mean time between occurring of scattering of electrons. Since there is no scattering of electrons in superconductors and the second term on the right side of equation can be ignored as $\boldsymbol{\tau}$ goes to infinity. And equation becomes

$$m\frac{d\mathbf{v}}{dt} = e\mathbf{E} \tag{2.3}$$

And the superconducting current density can be written as

$$J_s = n_s e \mathrm{v}_s \tag{2.4}$$

Where n_s is the electron density in superconductor and v_s is the average velocity of electrons. Then substitution of equation (2.4) into equation (2.3) gives us

$$\mathbf{E}=\frac{d}{dt}\left[\frac{m}{n_s e^2}\boldsymbol{j}_s\right] \tag{2.5}$$

$$\mathbf{E}=\frac{d}{dt}(\Lambda \boldsymbol{j}_s) \tag{2.6}$$

$$\Lambda=m/(n_s e^2) \tag{2.7}$$

Equation 2.6 is known as the first London equation.

In order to formulate the second London equation, it is possible to start by taking curl of Ampère's Law

$$-\nabla^2\mathbf{H}=\nabla\times\mathbf{J} \tag{2.8}$$

Then if derivative of equation (2.8) is combined with equation (2.6), it becomes

$$-\nabla^2 \frac{\partial \mathbf{H}}{\partial t} = \nabla \times \mathbf{E} \cdot \frac{1}{\Lambda} \tag{2.9}$$

Applying Maxwell Faraday equation into (2.9) gives

$$-\nabla^2 \frac{\partial \mathbf{H}}{\partial t} = -\frac{\partial \mathbf{B}}{\partial t} \cdot \frac{1}{\Lambda} \tag{2.10}$$

For a stationary field equation (2.10) yields to

$$\nabla^2 \mathbf{H} = \frac{\mathbf{B}}{\Lambda} \tag{2.11}$$

If vector identity $-\nabla^2\mathbf{H}=\nabla\times\nabla\times\mathbf{H}$ is applied and Ampère's Law is substituted into this equation it results with

$$\nabla \times \mathbf{J} = \frac{-\mathbf{B}}{\Lambda} \tag{2.12}$$

Which is known as second London Equation.

If the equation 2.11 is solved for different situations, it gives a characteristic length λ,

$$\lambda = \sqrt{\frac{\Lambda}{\mu_0}} \tag{2.13}$$

This is known as London Penetration Depth. It defines how much a magnetic field can penetrate into a superconductor.[10]

2.4 Ginzburg Landau Theory

The Ginzburg-Landau Theory is also formulated to describe superconductivity on a phenomenological level. But it uses quantum mechanical approach to describe the superconductivity phenomena. The idea is that; since there is no resistance to superconductive electrons, they can behave coherently over long range, and we can describe all electrons in superconducting sample by a single wavefunction $\boldsymbol{\psi}(\mathbf{r})$ and density of electrons in superconductor can be written as $n_s = |\boldsymbol{\psi}(\mathbf{r})|^2$

London equations can be verified by using the description given by Ginzburg-Landau theory. If Schrodinger equation in the presence of magnetic field is used the probabilistic current density in superconductor can be written by substituting the wavefunction for superconductive electrons described by Ginzburg-Landau theory into the Schrodinger equation. And this helps to find out the second London equation. By using Maxwell faraday law and second London equation first London equation can be verified.

Ginzburg-Landau theory also introduces the effects of fields strong enough to change the superconductive electron density and the new characteristic length $\zeta(T)$ which is called Coherence Length.

Ginzburg-Landau parameter $\kappa = \lambda/\zeta$ is also used to describe the type of the superconductor. Superconductors can be separated into two types by this parameter. For Type I superconductors Ginzburg-Landau parameter is lower than one.[11]

2.5 BCS Theory

The London and Ginzburg-Landau theories are formulated to describe the superconductivity based on observed phenomena but they don't give information about the physics of superconductors and they don't explain why the superconducting electrons don't face with any resistance below their transition temperature. This explanation is given by the BSC theory.

BSC theory introduces the formation of cooper pairs the temperatures below the transition temperature, T_c. Cooper pairs are defined by two electrons bound by attractive forces caused by phonon-electron interactions. These electrons have opposite spin direction yields the total spin of the cooper pairs to be zero. Therefore Cooper pairs are represented as bosons. At lower temperatures when phonons are decreased drastically cooper pair is formed while an electron creates a phonon and it is absorbed by the second electron. [9]

2.6 Type 2 Superconductors

Abrikosov found that some superconductors behave differently when they are subjected to an external magnetic field. Instead of losing superconductivity above critical magnetic field they are partially penetrated by magnetic flux up to higher level of magnetic field which superconductivity disappears. They are called as type II superconductors and they generally have Ginzburg-Landau parameter greater than 1. Separation between type I and type II superconductors for Ginzburg-Landau parameter is given as $\kappa = 1/\sqrt{2}$.

In type II superconductors, magnetic field penetrates into superconductor as vortices starting from the lower critical magnetic field, H_{c1} then density of vortices increase up to upper critical nagnetic field, H_{c2} where vortices overlap each other and superconductivity disappears. Each vortex has magnetic flux in its interior region which is exact integer multiple of certain value. This certain value is called magnetic flux quantum. H_{c2} values for type two superconductors are generally much larger than critical magnetic field values for type one superconductors.[9]

Chapter 3

Theory of Josephson Junctions and SQUIDs

Josephson Junction is the two superconducting electrode separated by an insulating layer which is named after Brian David Josephson. He was awarded with Nobel Prize for his predictions and calculations of electron tunneling between two superconducting samples. His discovery about supercurrent through potential barrier was verified by experimentalist after one year.[10] These discoveries had let many applications. One of them is Superconducting Quantum Interference Devices usually as known as SQUID. A SQUID is made of two josephson junction around a superconducting loop that supercurrent can tunnel across these junctions.[10] An aplied magnetic field cause phase change around loop and this cause the fluctuations in the current across SQUID. This quantum mechanical effect is used to detect very small magnetic field as small fractions of flux quantum.[12] In this chapter the theory behind SQUID was considered and information about how quantum mechanical phenomenon makes SQUIDs to capable to detect small magnetic fields was given.

3.1 Cooper Pairs and Macroscopic Wavefunction

In superconductors two electrons move together by attracting the crystal lattice when the lattice vibrations is very small at very low temperatures. These two electrons are called Cooper pairs and they move in the superconductors without any resistance.[13] Each Cooper pair has mass and charge of twice of an electron and the density of Cooper pairs is half of density of electrons. [10]
These cooper pairs can be represented by a wavefunction. Because of phase coherence of cooper pairs in superconductors all Cooper pairs can be represented by single wavefunction which is called as macroscopic wavefunction (Equation 3.1). [10]

$$\psi(\mathbf{r},t) = \sqrt{n^*(\mathbf{r},t)}e^{i\theta(\mathbf{r},t)} \tag{3.1}$$

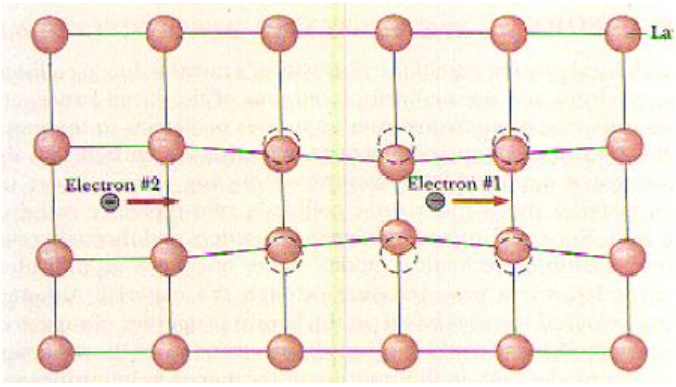

$$m^\star = 2m_e$$
$$q^\star = 2q_e$$
$$n^\star = \frac{n}{2}$$

Figure 3.1: Cooper pairs [10]

3.2 Current Density in Superconductor

The current density could be expressed by using wavefunction of the object (Equation 3.2), and the equation for current density in superconductor could be demonstrated by using macroscopic wavefunction of Cooper pairs where **A** is the magnetic vector potential. (Equation 3.3)[10]

$$\mathbf{J}_\mathrm{s} = q^*\mathrm{Re}\left\{\psi^*\left(\frac{\hbar}{im^*}\nabla - \frac{q^*}{m^*}\mathbf{A}\right)\right\} \tag{3.2}$$

$$\mathbf{J}_\mathrm{s} = q^*n^*(\mathbf{r},t)\left(\frac{\hbar}{im^*}\nabla\theta(\mathbf{r},t) - \frac{q^*}{m^*}\mathbf{A}(\mathbf{r},t)\right) \tag{3.3}$$

When the current density is written in presence of magnetic field, gauge transformations for magnetic vector potential (Equation 3.4) and magnetic scalar potential (Equation 3.5) can be used.

$$A' \equiv A + \nabla_\chi \tag{3.4}$$

$$\phi' \equiv \phi - \frac{\partial \chi}{\partial t} \tag{3.5}$$

and phase becomes;

$$\theta' = \theta + \frac{q^*}{\hbar}\chi \tag{3.6}$$

Current density for new gauge is;

$$\mathbf{J}_s = q^* n^*(\mathbf{r},t)\left(\frac{\hbar}{m^*}\nabla\theta'(\mathbf{r},t) - \frac{q^*}{m^*}\mathbf{A}'(\mathbf{r},t)\right) \tag{3.7}$$

3.3 Flux Quantization

In a superconductor ring total phase change around the loop must be an integer multiple of 2π. The equation for phase change around the loop can be written and this yields to quantization of magnetic flux.

$$\oint (\Lambda \mathbf{J}_s)\cdot dl + \int \mathbf{B}\cdot ds = n\Phi_0 \tag{3.8}$$

$$\Phi_0 = \frac{h}{2e} = 2.07\times 10^{-15}\mathrm{T}-\mathrm{m}^2 \tag{3.9}$$

3.4 Josephson Tunneling

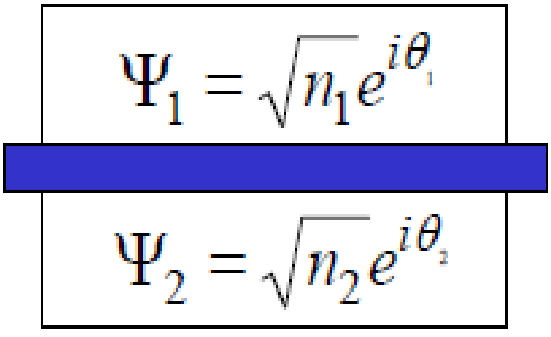

Josephson relations:

$$I = I_c \sin\varphi$$

$$V = \frac{\Phi_0}{2\pi}\frac{d\varphi}{dt}$$

$$\varphi = \theta_2 - \theta_1$$

Figure 3.2: Josephson junctions and voltage and current relations [10]

In josephson junctions two superconducting sample is separated by an non-superconducting region. Each superconducting sample can be represented by different wavefunction. Tunneling of cooper pair occurs in the non-superconducting region according to quantum mechanical tunneling of objects.

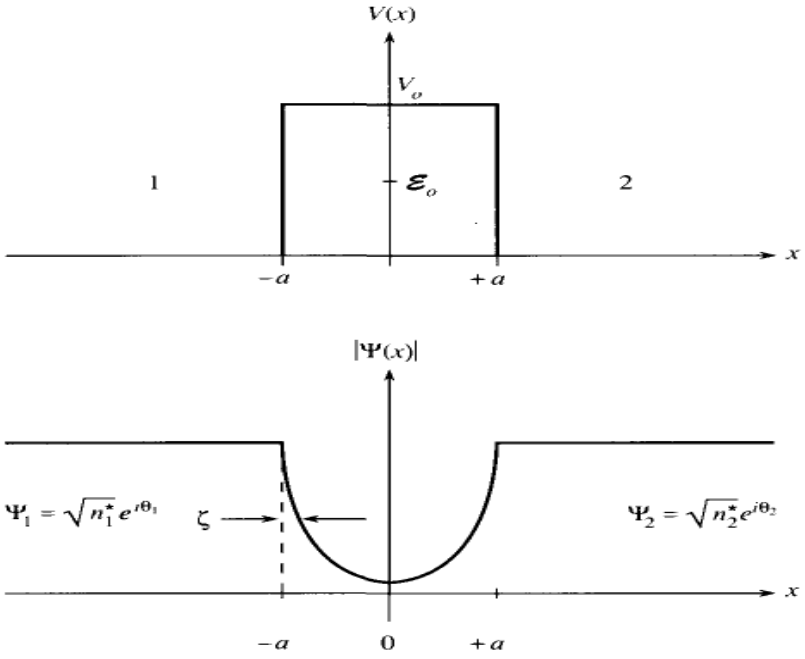

Figure 3.3: Potential and wavefunction across Josephson junction [10]

Wavefunctions for two superconducting regions are known and the wavefunction for insulating region can be written as sum of exponentially raising and decaying functions. [10]

$$\psi(x) = C_1 \cosh\left(\frac{x}{\zeta}\right) + C_2 \sinh\left(\frac{x}{\zeta}\right)$$
$$\zeta = \sqrt{\frac{\hbar^2}{2m^*(V_0 - \mathcal{E}_0)}} \tag{3.10}$$

Boundary conditions can be applied in order to solve the (equation 10) for C1 and C2.

$$\psi(-a) = \sqrt{n_1^*}e^{i\theta_1}$$
$$\sqrt{n_1^*}e^{i\theta_1} = C_1\cosh(a/\zeta) - C_2\sinh(a/\zeta) \tag{3.11}$$

$$\psi(+a) = \sqrt{n_2^*}e^{i\theta_2}$$
$$\sqrt{n_2^*}e^{i\theta_2} = C_1\cosh(a/\zeta) + C_2\sinh(a/\zeta) \tag{3.12}$$

C_1 and C_2 becomes;

$$C_1 = \frac{\sqrt{n_1^*}e^{i\theta_1} + \sqrt{n_2^*}e^{i\theta_2}}{2\cosh(a/\zeta)} \tag{3.13}$$

$$C_2 = \frac{\sqrt{n_1^*}e^{i\theta_1} - \sqrt{n_2^*}e^{i\theta_2}}{2\sinh(a/\zeta)} \tag{3.14}$$

Now everything is known to write down the current density across Josephson junction. By using current density formula (Equation 3.2) and wavefunction for junction (Equation 3.10), current density can be simply written down the in terms of C1 and C2. [10]

$$\mathbf{J_s} = \frac{q^*\hbar}{m^*\zeta}\mathrm{Im}\{{C_1}^* C_2\} \tag{3.15}$$

When we substitute C1 and C2 (Equation 3.15) becomes;

$$\mathbf{J_s} = -\frac{q^*\hbar}{m^*\zeta}\frac{\sqrt{n_1^* n_2^*}}{2\sinh(a/\zeta)\cosh(a/\zeta)}\sin(\theta_1 - \theta_2) \tag{3.16}$$

By using the Josephson current relation the equation for critical current of junction can be written.

$$J_c = \frac{e\hbar\sqrt{n_1 n_2}}{2m\zeta\sinh(2a/\zeta)} \tag{3.17}$$

3.5 DC SQUID

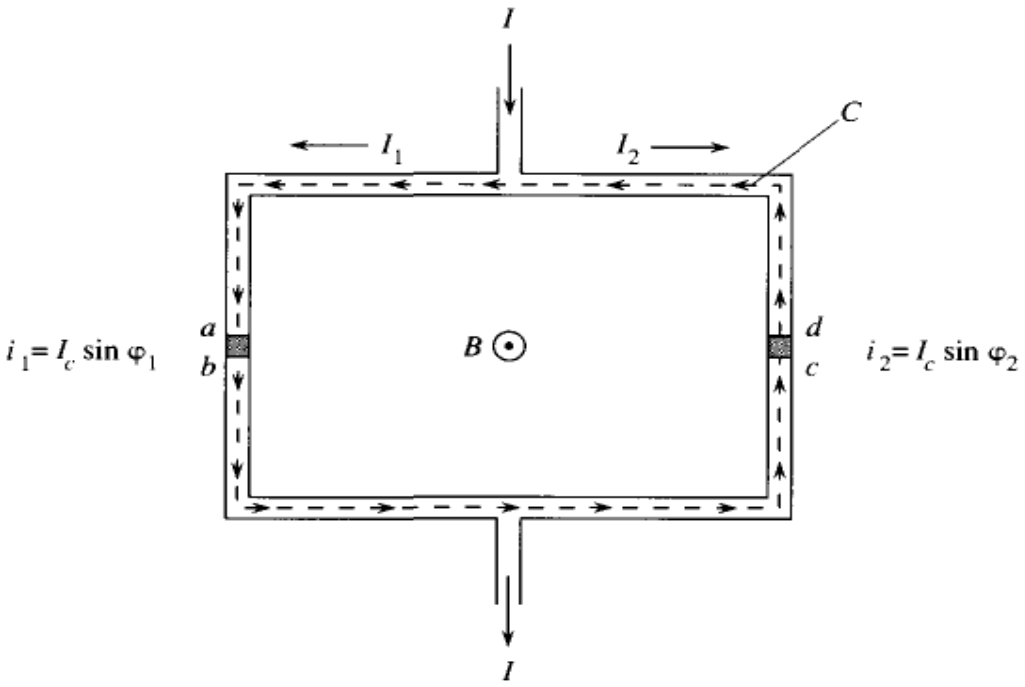

Figure 3.4: Schematic Representation of SQUID [2]

SQUID has a superconducting loop and Josephson junctions on each arm of loop as shown as Figure 3.4. Current across the SQUID can be written as sum of the currents on two junctions (Equation 3.18). The current across the SQUID depends on the phase difference on each junction.

$$i = i_1 + i_2 = I_c \sin\varphi_1 + I_c \sin\varphi_2 = 2I_c \cos\left(\frac{\varphi_1 - \varphi_2}{2}\right) \sin\left(\frac{\varphi_1 + \varphi_2}{2}\right) \tag{3.18}$$

Phase difference around the loop can be written as;

$$\oint \nabla\theta \cdot d\mathbf{l} = 2\pi n = (\theta_b - \theta_a) + (\theta_c - \theta_b) + (\theta_d - \theta_c) + (\theta_a - \theta_d) \tag{3.19}$$

Phase differences in the junctions and superconducting wires can be written as;

$$\theta_b - \theta_a = -\varphi_1 - \frac{2\pi}{\Phi_0}\int_a^b \mathbf{A}\cdot d\mathbf{l} \tag{3.20}$$

$$\theta_d - \theta_c = \varphi_2 - \frac{2\pi}{\Phi_0}\int_c^d \mathbf{A}\cdot d\mathbf{l} \tag{3.21}$$

$$\theta_c - \theta_b = \int_b^c \nabla\theta\cdot d\mathbf{l} = -\Lambda\int_b^c \mathbf{J}\cdot d\mathbf{l} - \frac{2\pi}{\Phi_0}\int_c^d \mathbf{A}\cdot d\mathbf{l} \tag{3.22}$$

$$\theta_a - \theta_d = \int_d^a \nabla\theta\cdot d\mathbf{l} = -\Lambda\int_d^a \mathbf{J}\cdot d\mathbf{l} - \frac{2\pi}{\Phi_0}\int_d^a \mathbf{A}\cdot d\mathbf{l} \tag{3.23}$$

If equations (3.20), (3.21), (3.22), and (3.23) are substituted into equation (3.19), it results with the equation (3.24).

$$\varphi_2 - \varphi_1 = 2\pi n + \frac{2\pi}{\Phi_0}\oint \mathbf{A}\cdot d\mathbf{l} + \frac{2\pi}{\Phi_0}\int_b^c \Lambda\mathbf{J}\cdot d\mathbf{l} + \frac{2\pi}{\Phi_0}\int_d^a \Lambda\mathbf{J}\cdot d\mathbf{l} \tag{3.24}$$

The integral in the second term of equation (3.24) is the total magnetic flux inside the loop by external magnetic field. Then equation (3.24) becomes;

$$\varphi_2 - \varphi_1 = 2\pi n + \frac{2\pi\Phi}{\Phi_0} + \frac{2\pi}{\Phi_0}\int_{C'} \Lambda\mathbf{J}\cdot d\mathbf{l} \tag{3.25}$$

The integration of **J** around the loop but excluding the junctions can be negligible [10].

$$\varphi_2 - \varphi_1 = 2\pi n + \frac{2\pi\Phi}{\Phi_0} \tag{3.26}$$

if the equation (3.26) is substituted into equation (3.18), current across SQUID becomes;

$$i = 2I_c \cos\left(\frac{\pi\Phi}{\Phi_0}\right)\sin\left(\varphi_1 + \frac{\pi\Phi}{\Phi_0}\right) \tag{3.27}$$

If derivative of equation (3.27) is taken, maximums occur at;

$$\cos\left(\varphi_1 + \frac{\pi\Phi_{\text{ext}}}{\Phi_0}\right) = 0$$

At this point;

$$\sin\left(\varphi_1 + \frac{\pi\Phi_{\text{ext}}}{\Phi_0}\right) = \pm 1$$

Using these relations maximum current across SQUID can be written as;

$$i_{\max} = 2I_c \left|\cos\left(\frac{\pi\Phi_{\text{ext}}}{\Phi_0}\right)\right| \tag{3.28}$$

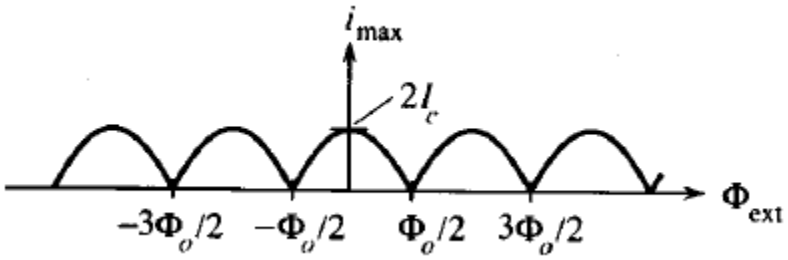

Figure 3.5: Current across SQUID as a function of applied magnetic flux. [10]

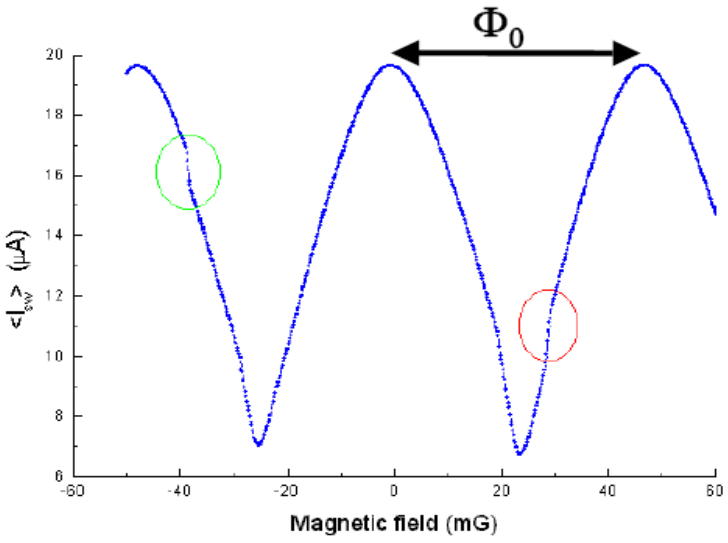

Figure 3.6: Actual measurement result with SQUID [10]

3.6 Summary

In this chapter theoretical background of Josephson Junctions and magnetic field sensing with SQUID were reviewed. SQUID behaves like magnetic flux to current convertor as seen as Figure 3.5 and 3.6. Period of fluctuations on current is equal to flux quantum. That means magnetic flux can be detected as small fractions of flux quantum. As a consequence of this fact SQUIDs are most sensitive detectors of magnetic field. There is no limit but quantum limit for sensitivity of SQUID.[14] Sensitivity of SQUID is reduced as the noise level of current increases. Noise level is depend on material properties of superconductors used and the design of device.[14] In order the increase the sensitivity, design and fabrication process of device is most important factor.[15]

Chapter 4

Review of HTS Josephson Junctions

Josephson junction is based on quantum mechanical tunneling of electrons between weakly coupled two superconducting regions. Its unique properties make it a building block for future superconducting electronic circuits. Josephson junctions are key element for various applications such as Rapid Single Flux Quantum (RSFQ) logic circuits, Superconducting Quantum Interference Devices(SQUID), terahertz applications, Single Electron Transistors etc. After discovery of high temperature superconducting (HTS) materials which operates above liquid nitrogen temperature, implementations of Josephson junctions became more important for development of practical devices. Although application of Josephson junctions are very promising for future high speed computers based on RSFQ logic and Quantum information Processing Devices, fabrication technology for HTS Josephson junctions is still in its childhood. Well defined and integrable fabrication technology is needed for commercialization of these technologies. In this chapter we will talk about different types of Josephson junctions and implementations of them by current micro and nanofabrication technologies. Current methods for Josephson junction fabrication will be reviewed and future projections will be discussed.

4.1 Introduction

Josephson Junctions take its name from Brian David Josephson who predicted the quantum mechanical tunneling of supercurrent trough weak link between two superconducting regions. One year later his predictions were verified by experimentalist at IBM research center. Josephson and they were awarded by Nobel Prize at 1973. Josephson Effect is completely depending on quantum

mechanical behavior of cooper pairs along junctions between weakly coupled two superconducting regions. This phenomenon leads to invention of different kinds of superconducting electronic devices. Josephson Junctions are used in implementation of superconducting qubits which is essential building block of quantum information processing devices, Superconducting quantum interference devices (SQUID) which is capable of making measurements with extreme sensitivity, Rapid single flux quantum (RSFQ) logic circuits which is very promising devices for future generation of microprocessors with clock speed higher than 100 GHz, terahertz detectors, Single electron transistors etc. Most of these applications are critical for improvement of today's integrated circuit industry while feature sizes of devices are becoming much smaller every year. But the important thing is the integration of these technologies with the current semiconductor industry. In order to commercialize these technologies based on Josephson junctions we have to find straightforward fabrication methods and these methods have to be easily adapted to IC industry. With the invention of high temperature superconducting materials interest in superconducting circuits started to increase rapidly. Because the critical temperature of the HTS materials are above the liquid nitrogen temperature and they are commercially available and cheaper when compared to liquid helium temperature. But the fabrications of HTS Josephson junctions are more difficult than the older Josephson junctions fabricated with low temperature superconductors. Low temperature superconductors are metals like Aluminum and Niobium which are fabrication process are well defined in IC industry. Unfortunately, comparable technology doesn't exist for high temperature materials for the following reasons: First in contrast to metals high temperature superconductors need to be grown epitaxially which requires careful choice of materials and processing techniques.

Secondly superconductor coherence length is short an highly anisotropic. As a result of this, material properties of high temperature superconductors are highly susceptible to chemical changes in

atomic scale and superconducting properties at the interfaces can easily be suppressed at the junction interfaces. This really decreases the performance of the Josephson junctions. Thus the superconductor need to have perfect crystallization and perfectly defined interface has to be formed at the level of single unit cell. Thirdly the oxide barrier materials have complex crystal structures and they are strongly sensitive to defects on atomic length scale. As a result transport across barriers is strongly affected by imperfections in the barrier and the interfaces with superconductor electrodes. Thus perfect crystalline quality and homogeneity is required for barriers.[1]

In order to develop and commercialize the HTS microelectronics technology epitaxial multilayer device technology is required. This technology has to meet several criteria. The junctions must have necessary electrical properties. Resistively shunted junction (RJS) characteristics are necessary for most of the applications. Critical current and resistance must be in suitable ranges. Parasitic inductance and capacitance must be acceptably small.[16] These are major concerns for Josephson junction devices. Importance and these parameters are significantly increases with the circuit complexity. In several years after discovery of high temperature superconductivity attempts to fabricate Josephson junctions were failed because of the different properties of HTS materials which prevent to use of low temperature circuit technology to these materials. But since that time significant improvements on HTS junction technology is observed with the use of advanced micro and nanofabrication technologies. Nowadays there are several fabrication methods for HTS Josephson junctions. There are some advantages and disadvantages of these methods over each other. They are favorable for different kind of applications. But there is still need for development of straightforward fabrication technology for HTS micro and nanoelectronic circuits.

In this chapter different types of HTS Josephson junctions and their fabrication process were reviewed and future possibilities for HTS electronic devices were discussed.

4.2 HTS Josephson Junction Fabrication Technology

Fabrication of HTS Josephson junctions is mostly depending on following technologies:

-Fully epitaxial thin film growth,

-Processing of multilayer structures including lithography, patterning techniques and metallization,

-Interface control and engineering on an atomic scale,

-Controlled deposition of spatially homogeneous barrier layers.[17]

Within the last two decades a tremendous progress has been evolved in the fabrication of heteroepitaxial layer structures. As mentioned before engineering of interface and barrier layers are key point of fabrication of HTS Josephson junctions. Due to importance of interfaces HTS Josephson junctions can be classified according to their type of junction interfaces.

4.2.1 Junctions without interfaces

Constriction type junctions such as weakened structures junctions and nanobridges where the weak coupling is obtained by locally degrading the superconducting properties of thin films.[17] This can be achieved by focused electron or ion beam irradiation of superconducting nanobridges that results only weakening of superconductor without interface.[18] This weakening can also be done by ion implantation.[19] This is a single layer technology and fabrication is easier.

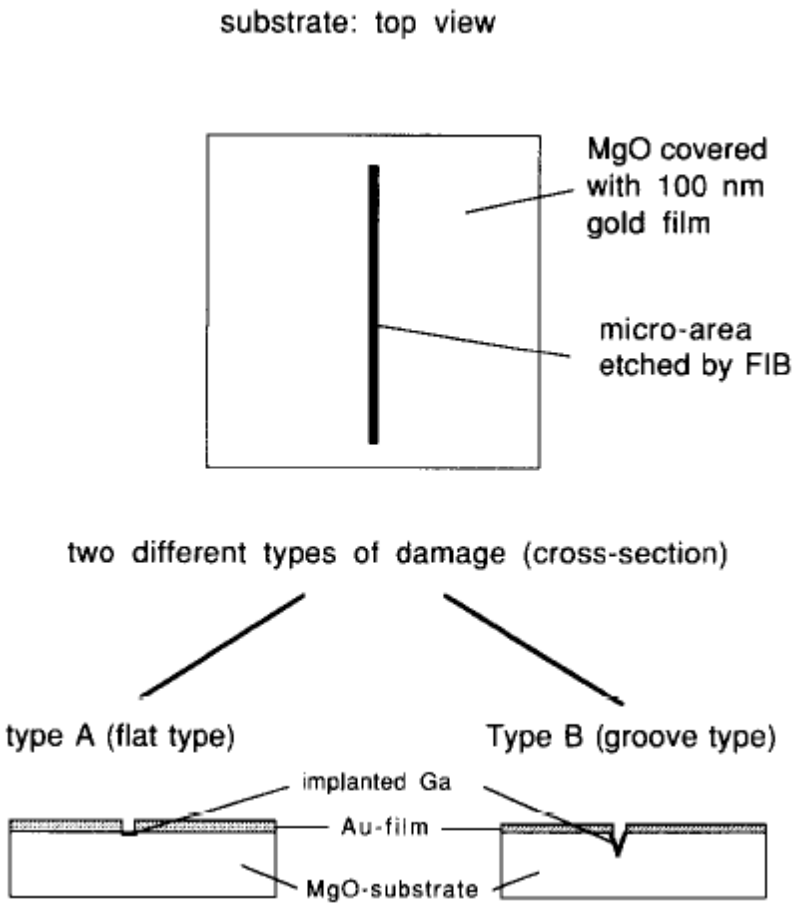

Figure 4.1: FIB formation of Josephson Junction[19]

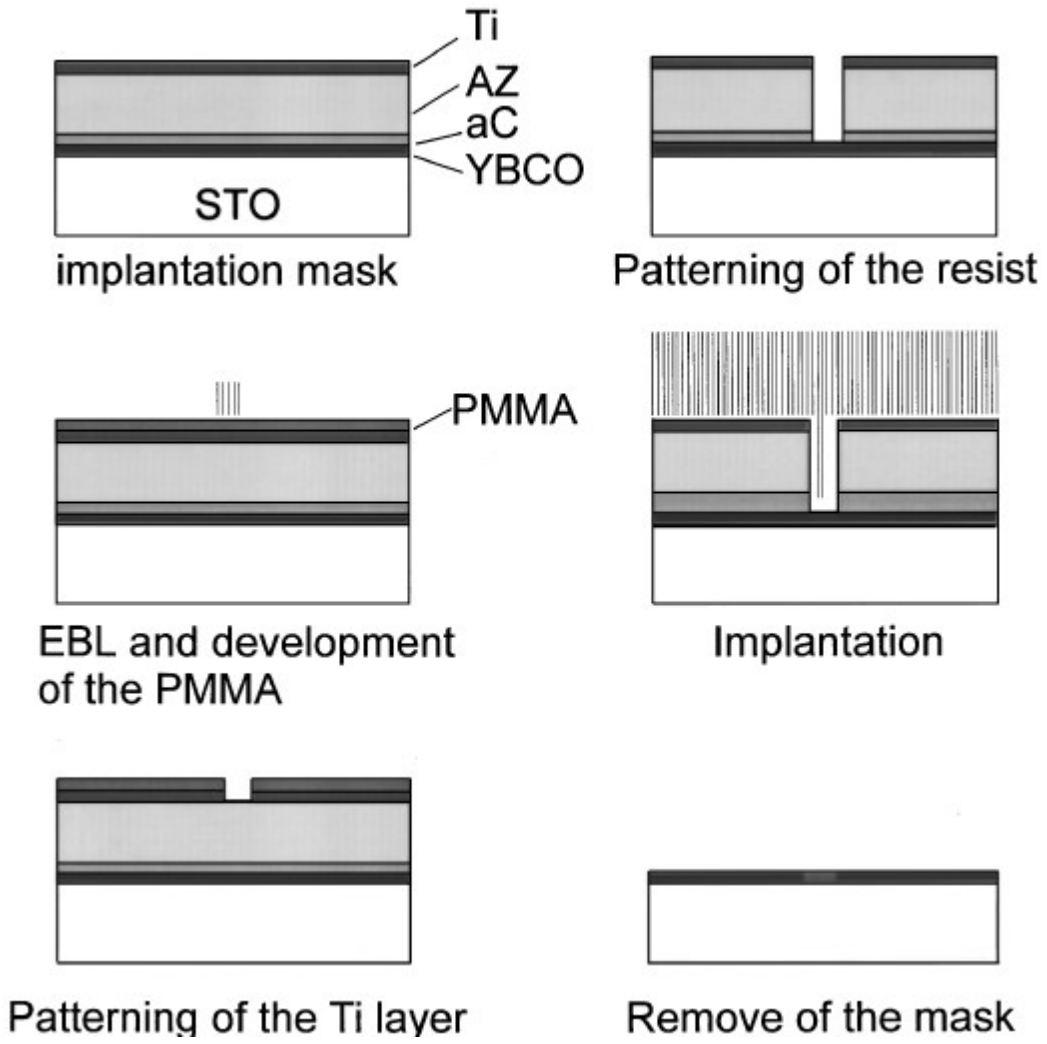

Figure 4.2: Junction formation by ion implantation[19]

4.2.2 Junctions with intrinsic interfaces:

Although the fabrication of Josephson junction with insulator barrier is difficult, HTS materials allows the fabrication of new type of Josephson junction based on intrinsic interfaces and barriers. The grain boundaries of superconducting thin films behave like weak links for circulating

supercurrent. This is not observed in metallic superconductors. These grain boundaries are used to fabricate Josephson junction by artificial positioning of them. This type of junctions include bicrystal grain boundary Josephson junctions (BC-GBJ) and step-edge grainboundary junctions (SE-GBJ).[17] In BC-GBJ epitaxially deposited film follows the grain boundaries on bicrystal substrate. The grain boundary angle and symetry is determined by the substrate. BC-GBJs have been fabricated using epitaxial YBCO and BSCCO superconducting thin films.[20] Also the other type of GBJ at steep substrate steps can be fabricated by epitaxial film deposition,[21] Biepitaxial GBJs(BE-GBJ) are another type of artificial GBJ which is fabricated by controlling the grain boundary angle.[22] At present the GBJs are the most studied and best understood HTS-JJs.

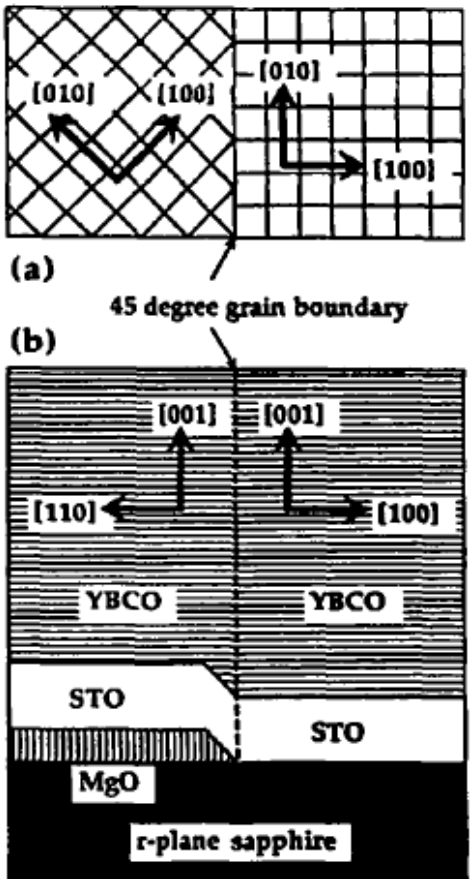

Figure 4.3: BE-GBJs [22]

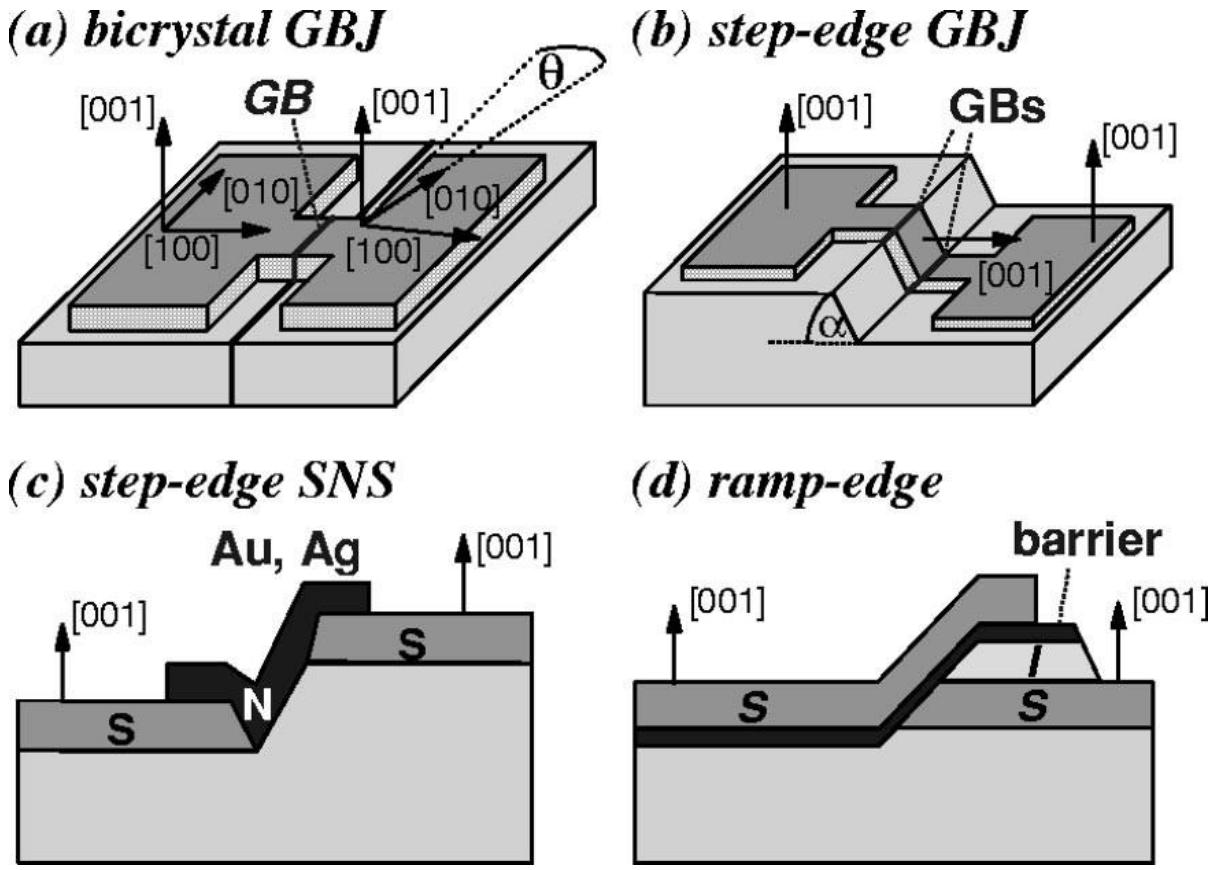

Figure 4.4: Most popular Josephson junction fabrication techniques [17]

4.2.3 Junctions with extrinsic interfaces:

In the fabrication of junctions based on the use of artificial insulator or nonsuperconducting barriers one has to deal with extrinsic interfaces between the HTS electrodes and the barrier material. Although this class is most successful for LTS, their controlled fabrication is difficult for HTS and requires the most advanced fabrication technology.[17] Ramp-edge SNS junctions (RE-SNS),[23] planar junctions(PJ)[24] and step-edge SNS junctions(SE-SNS)[25] are different type junctions in this category.

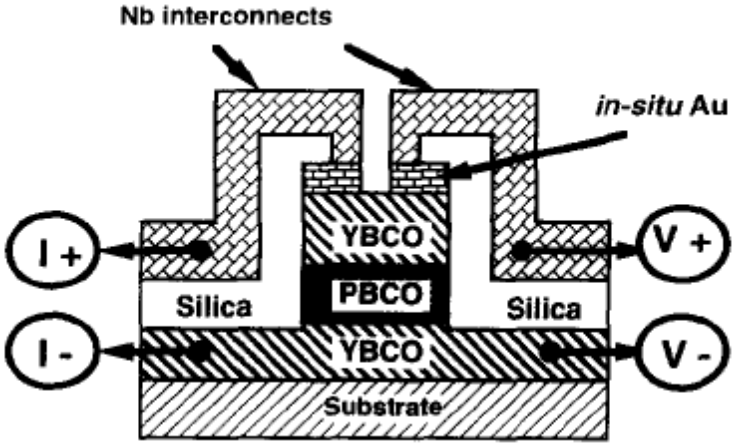

Figure 4.5: Schematic diagram of a Planar Junction [24]

There are lots of specific structures of Josephson junctions fabricated by different research groups around the world. But in the next pages the fabrication process of most popular type of Josephson junctions were reviewed in more detailed way.

4.3 Bicrystal grain-boundary junctions

Development of a useful HTS Josephson junction technology and the understanding of transport properties across grain boundaries was initiated by the pioneering work at IBM on BC-GBJs.[1] These junctions are fabricated by the epitaxial growth of HTS thin film on a bicrystal substrate with predetermined misorientation angle.[20]

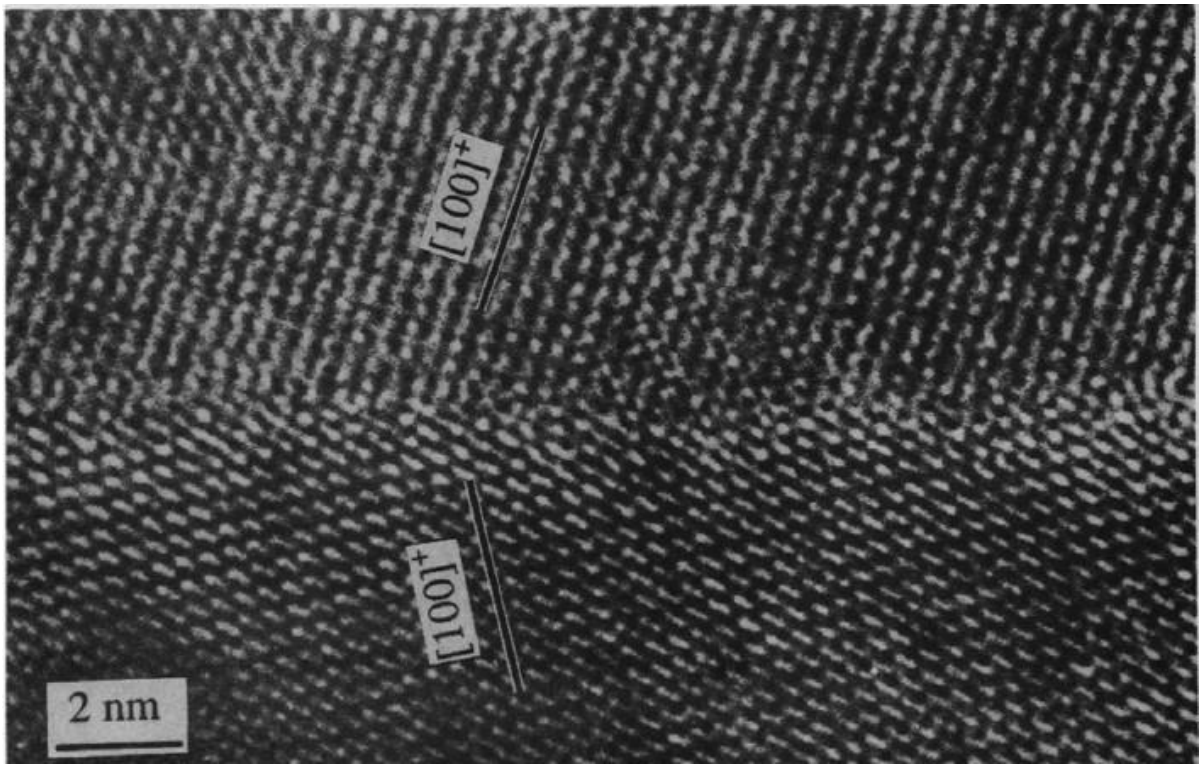

Figure 4.6: TEM image of grain boundary of HTS thin film[20]

Straightforward fabrication process of BCGBJs makes them most reliable and successful among the other types of josephson junctions. BC-GBJs can be used easily in aplications which doesn't require a lot of number of junction at arbitrary positions on the substrate. Substrates which supports epitaxial growth of HTS thin films is suitable for BC-GBJs, including SrTiO3, YSZ, Si, NdGaO3 , MgO, LaAlO3 and Sapphire. YBCO is used at most of the work on BCGBJs but other superconductors are also investigated including Bi2Sr2CaCu2O8, Tl2Ba2CaCu2O8, HgBa2CaCu2O6 and La1.85Sr0.15CuO4. [1]

4.4 Step-edge grain-boundary junctions

Step-edge GBJs are one of the widely used type of Josephson junctions. SE-GBJs are based on the fact that orientation of epitaxially grown HTS films changes at a steep step in the substrate or deposited dielectric material.[21] This technique is studied by several groups. Common substrate materials are SrTiO3 and LaAlO3.[1] For large step angles (a.70°) the two grain boundaries grow with different orientations.[21] The substrate steps are aligned along major cubic axes of the substrate, and are usually patterned by standard lithography and Ar-ion milling so that their location can be chosen at will.(Figure 7) This advantage over the bicrystal technique enables one to fabricate more complex circuits. Even for SQUIDs which require only one or two junctions, this flexibility in layout can be important, for example, for minimizing parasitic inductances. It has been proposed that the grain boundaries formed at step edges behave as junctions because of their defect structure (Herrmann et al., 1995), since 90° grain boundaries in planar films do not exhibit such behavior. Thus the properties of step edge junctions depend strongly on the microstructure of the milled step and on the film-growth conditions, leading to greater spreads in parameters than for bicrystal junctions. The use of carbon like diamond masks and very low milling rates improve the definition of the steps, and hence their reproducibility. [1]

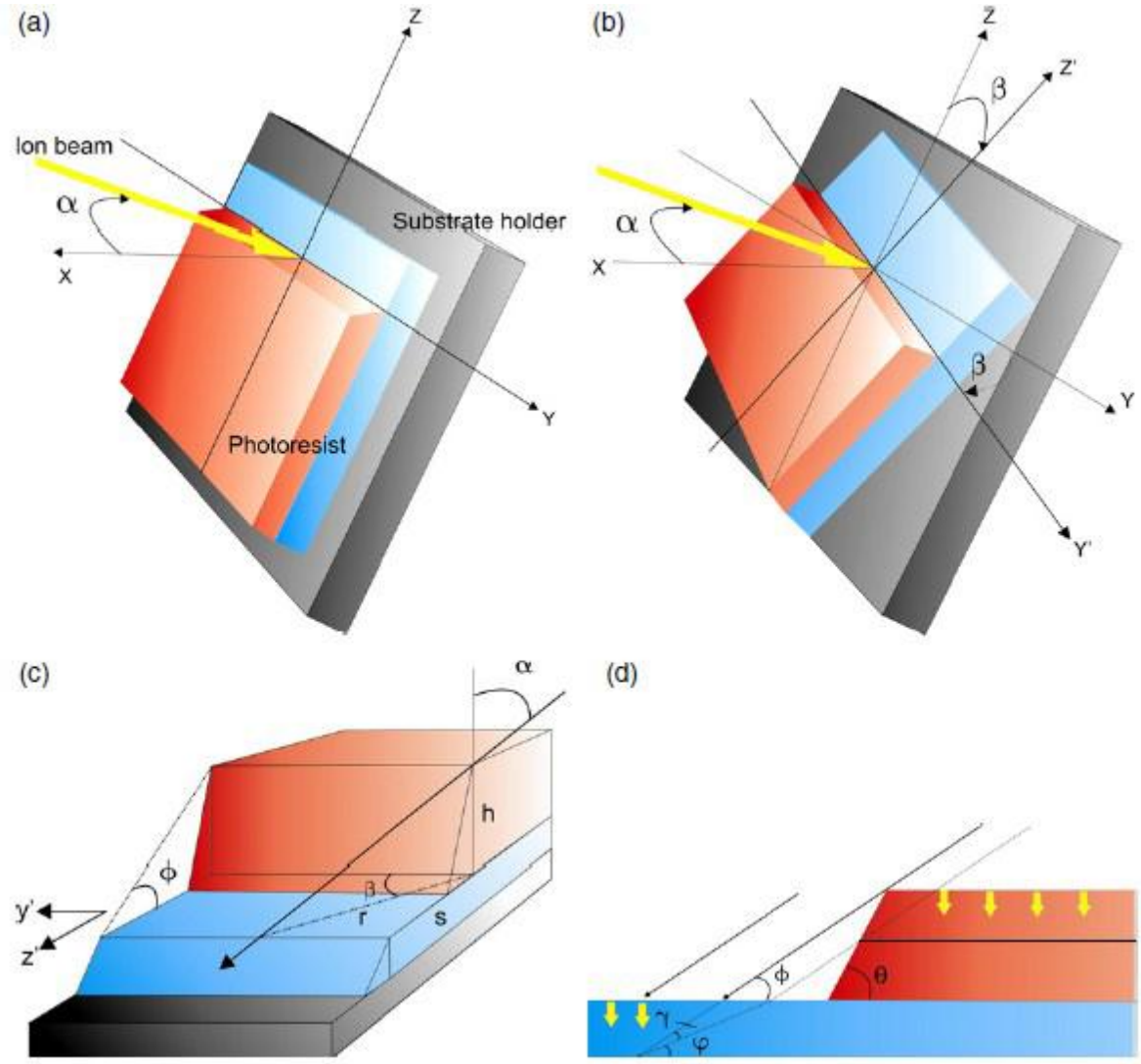

Figure 4.7: Model of step-edge process [21]

4.5 Step-edge SNS junctions

SNS junctions are widely used in low temperature superconducting circuit applications. In HTS materials fabrication process is somehow similar.[25] Firs a steep step is cut in the substrate 50-100 nm high by lithography and Argon ion milling and HTS thin film is deposited directionally so that

film doesn't grow on the step depend on the step angle and directionality of deposition process. The gap at the step can be filled by directional deposition of a gold or silver layer without breaking the vacuum. This layer makes contact to a-b plane of HTS films.[1] Transport and noise properties of SE-SNS junctions are not good as the GBJ. And the lack of control of the interface properties is a major problem for this kind of junctions. Because of these difficulties applications of this kind of junctions are not widespread as the other ones.

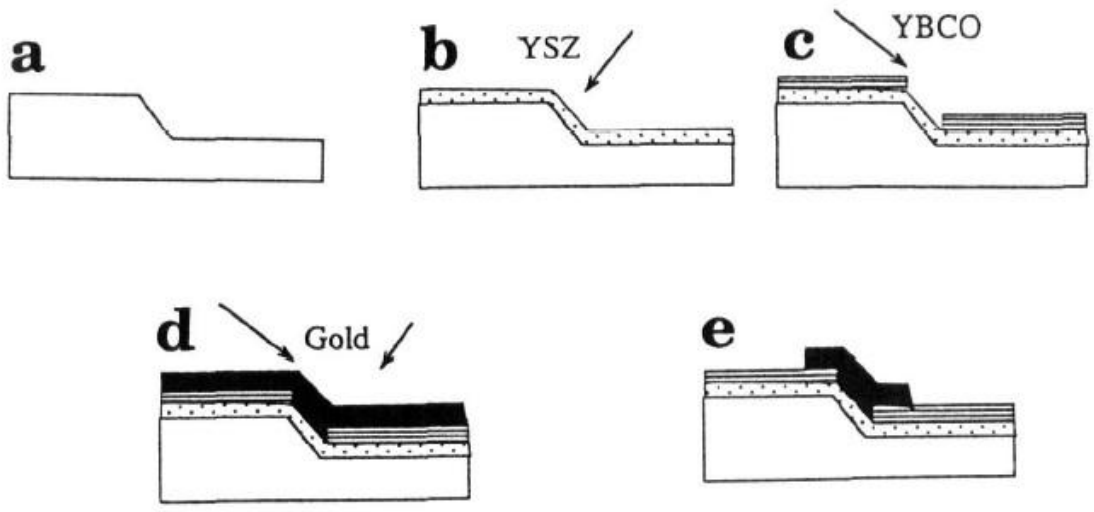

Figure 4.8: Schematic view of SE-SNS junction fabrication process [25]

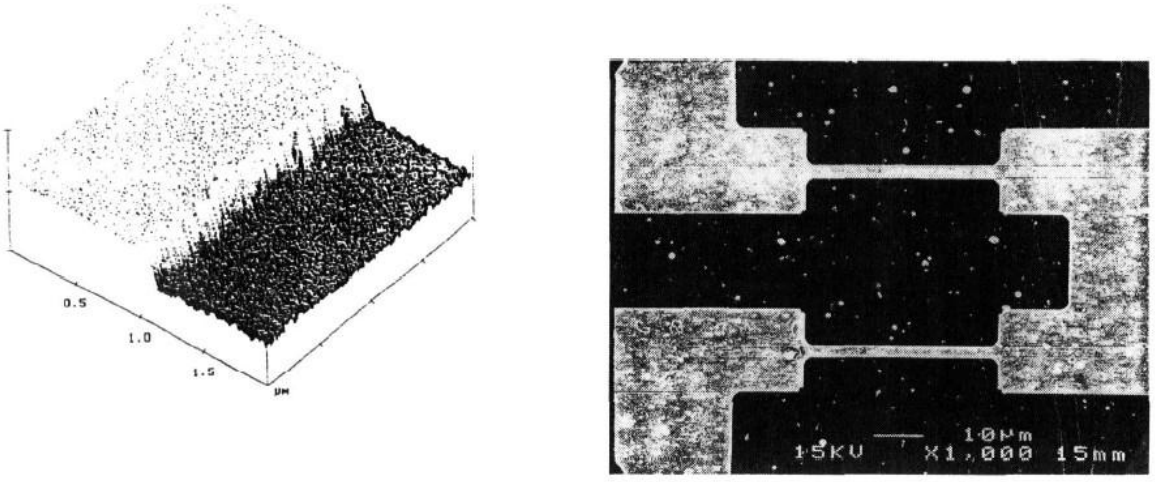

Figure 4.9: a) AFM picture of SE-SNS junction [25], **b)** SEM image of two SE-SNS junctions on a chip [25]

4.6 Ramp-edge SNS junctions

These junctions require the fabrication of an epitaxial trilayer with two superconducting electrodes separated by a thin barrier layer. Current transport is along the a-b planes of the c-axis oriented electrode films, taking advantage of the larger coherence length along this direction.[1] One fabricates a ramp edge junction by first depositing a YBCO film and covering it with a thick, insulating film. Next, one patterns a ramp with a shallow angle (typically 10° to 20°) using ion milling or anisotropic wet etching, and finally deposits the barrier material and top electrode in situ. The top electrode effectively shields the magnetic-field component normal to the film surface. Hence ramp-edge junctions may offer an important advantage over planar GBJ's for operation in magnetically unshielded environments. Furthermore, ramp edge junctions may be more robust against aging and thermal cycling compared to GBJ's since the barrier/interfaces are not directly exposed to the

environment.[1] The key requirement is a lower electrode with a smooth ramp edge of excellent crystalline quality to support the growth of a thin, homogenous barrier. Thus any damage caused by milling the ramp or by its exposure to air has to be healed prior to deposition of the barrier. The need to pattern the ramp with an ex situ process can be avoided by patterning the lower electrode with a micro shadow mask.[1]

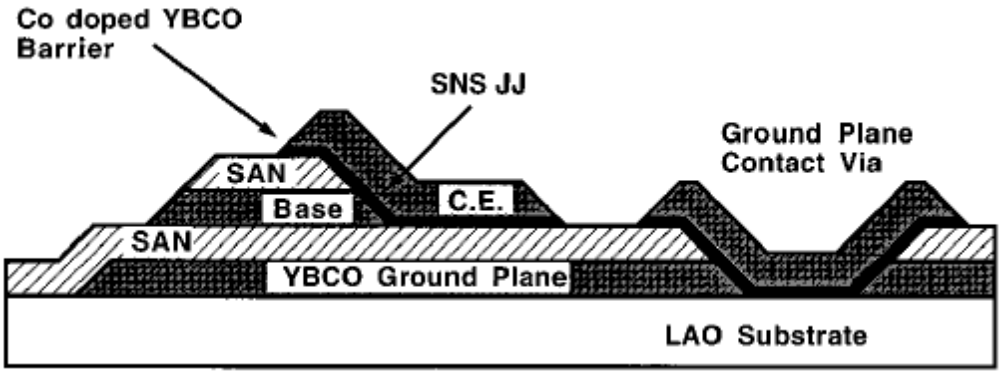

Figure 4.10: Schematic view of REJ [9]

4.7 Summary

After discovery of high temperature superconductors interest in fabrication of superconducting integrated circuits increased tremendously. There was a huge effort for the development of reliable fabrication techniques for Josephson junctions; because of they are building blocks of HTS electronic circuits. In this chapter fabrication technologies for high temperature superconducting Josephson junction were reviewed. There are really promising approaches for junction fabrication. But they have some advantages and disadvantages when compared the others. Standardization of these methods is needed for commercialization like semiconductor industry.

Chapter 5

Fabrication Procedure

Towards the completion of this thesis, fabrication procedures for nanoscale Josephson junctions and SQUIDs were investigated. Nanoscale SQUIDs offer very high magnetic flux sensitivity due to their ability to be coupled with small magnetic particles, low parasitic inductance, and low level of flux noise. And high temperature superconductors offer several advantages for use in SQUIDs. YBCO allows us to fabricate Josephson junctions on its intrinsic grain boundaries with advantageous parameters like high critical current density, comparably low level of flux noise, and low level of inductance. And it can be used at higher temperatures than liquid nitrogen and it can sustain superconductivity at higher magnetic fields. These advantages encourage researchers to develop SQUIDs with YBCO grain boundary junctions and submicron dimensions. Recently there has been several achievements on fabrication of nanoSQUIDs and patterning of YBCO nanowires.[3,4] But fully controllable, simple and straightforward fabrication technology has not been developed yet as semiconductor IC industry. In this work it is attempted to develop a new fabrication method for YBCO bi-crystal grain boundary Josephson Junctions and NanoSQUIDs.

In this work fabrication of nanoSQUIDs was realized by using electron beam patterning and physical dry etching of YBCO thin films on STO substrates. YBCO thin films were deposited using RF magnetron sputtering technique in the mixture of Ar and O_2 gases and annealing at high temperatures in O_2 atmosphere. Patterning of YBCO thin films was done by one Electron Beam Lithography step followed by Reactive Ion Etching and physical dry etching. First SiO_2 thin film was deposited on YBCO by RF magnetron sputtering and it was patterned by EBL using PS (Polystyrene)

as resist material and SiO_2 was etched by Reactive Ion Etching. Then SiO_2 was used as an etch mask for physical dry etching of YBCO and nanoscale patterns were formed on YBCO thin film.

Besides the patterning of YBCO thin films on nanoscale, alignment of these patterns on bi-crystal grain boundary is a big challenge for fabrication of nanoSQUIDs. Because, grain boundary of YBCO cannot be seen directly by Scanning Electron Microscope during e-beam lithography is performed. Only the defects along grain boundary can be seen. But the defects help to locate the grain boundary and allow us to do patterning aligned to grain boundary. And it is possible to make grain boundary more visible on SEM by dry etching of film to get grooved profile at grain boundary. This can be useful for alignment with better resolution. Also angled imaging of substrate makes grain boundary visible with higher resolution.

In this chapter, experimental procedure to deposit YBCO film by RF magnetron sputtering, characterization of them by Scanning Electron Microscopy (SEM) and Energy Dispersive X-Ray Spectroscopy (EDX) and patterning of YBCO thin films by e-beam lithography and physical dry etching was discussed.

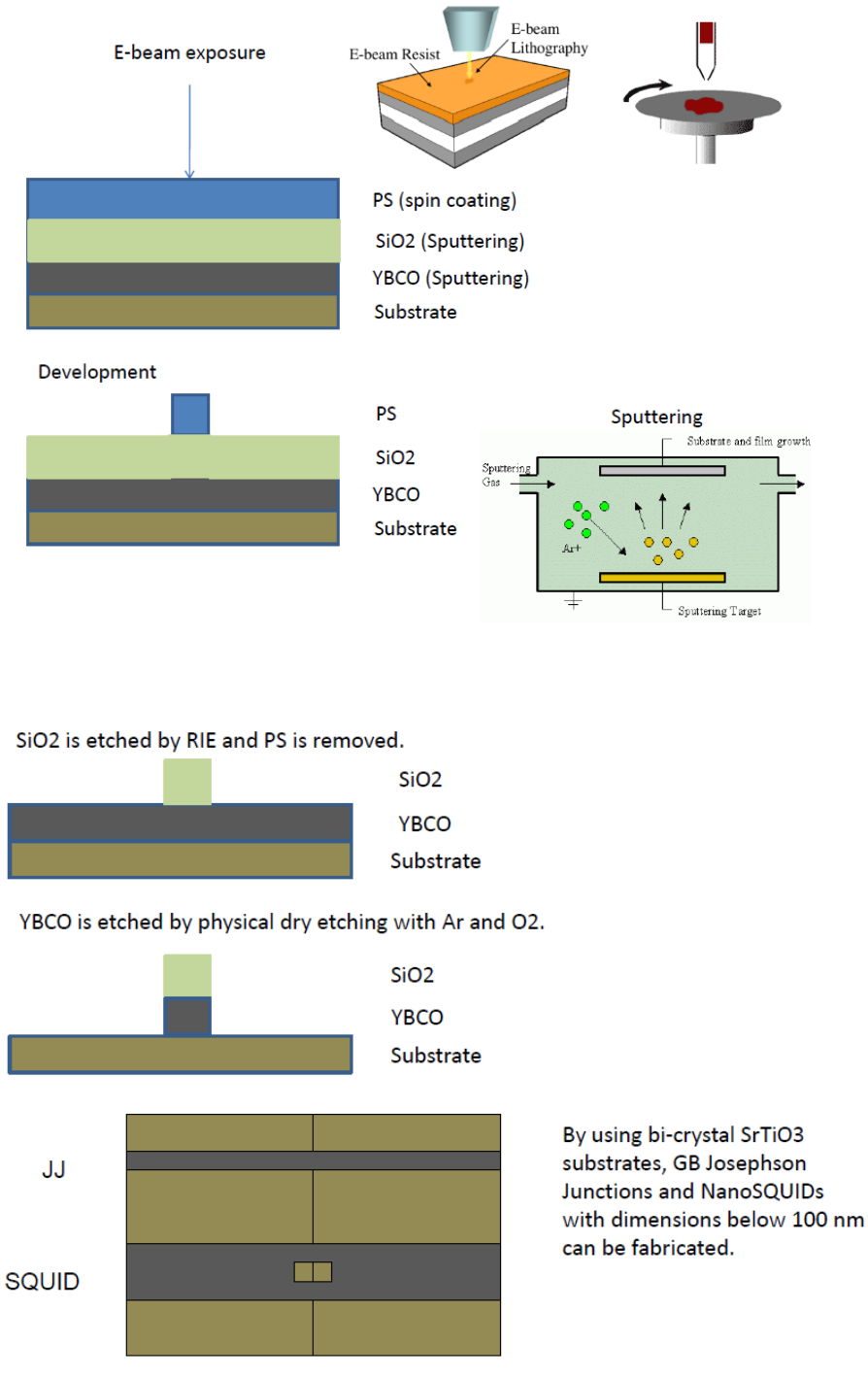

Figure 5.1: Schematic fabrication process for patterning of YBCO thin film.

5.1 Device Fabrication

The steps in fabrication process can be listed as follows:

- Substrate preparation and cleaning,
- YBCO thin film deposition,
- SiO_2 deposition,
- Spinning of PS as EBL Resist,
- E-beam exposure patterning,
- Etching of SiO_2 by RIE,
- Sputter etching of YBCO.

In the following sections details of each step will be discussed.

5.1.1 Film Deposition by RF Magnetron Sputtering

There are several techniques reported for deposition of YBCO thin films but Pulsed Laser Deposition and Sputtering are most popular ones among them.[1] In this work RF magnetron sputtering was used to deposit YBCO thin films on STO substrates. Grain Boundary on STO film was characterized prior to film deposition. Defects were clearly visible by SEM. Angled imaging of substrate is examined in order to see grain boundary by using the orientation difference between two crystals across. It helped

a little bit to locate the grain boundary with higher resolution.

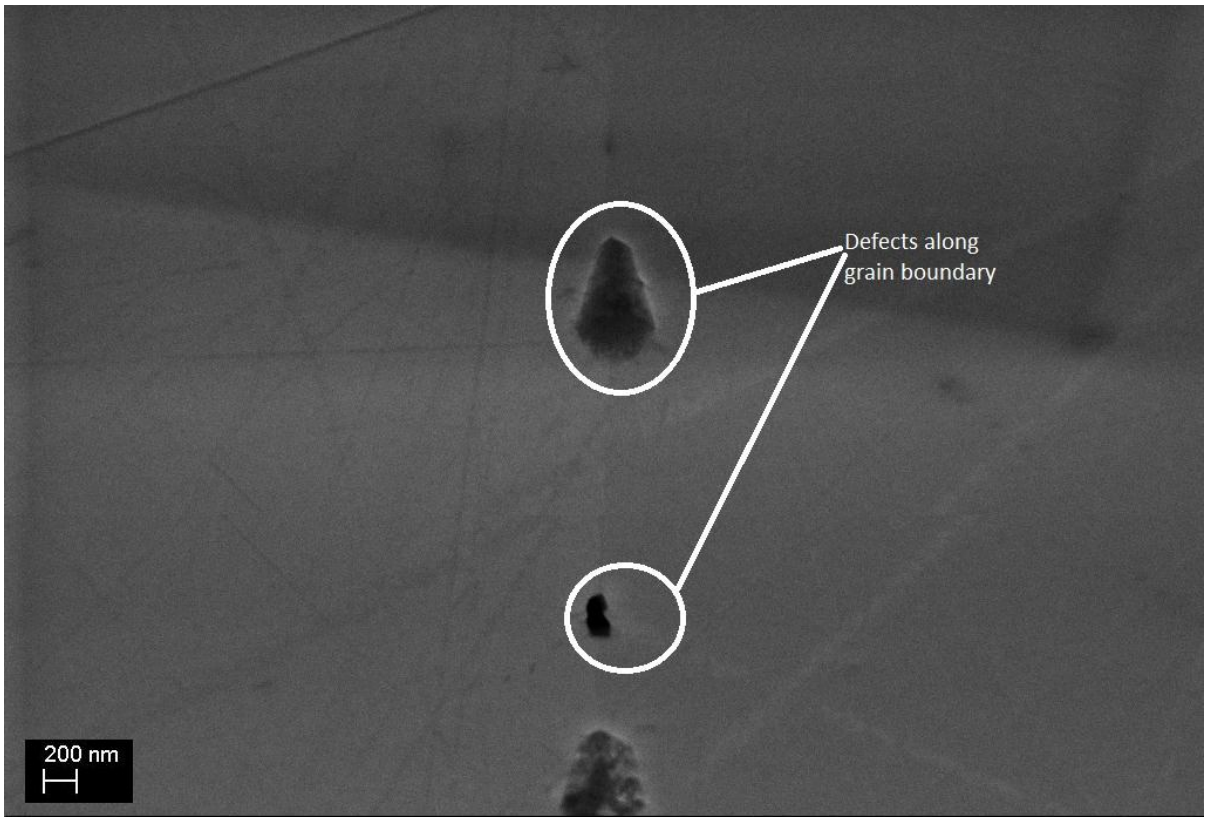

Figure 5.2: Grain Boundary of STO substrate

Prior to YBCO deposition substrates were cleaned using Acetone in ultrasonic bath and rinsed with Isopropanol. And substrates were cleaned with Argon plasma in sputtering chamber by applying the RF power to substrate holder. Ionized Argon atoms hit the substrates surface and etch the surface slowly to remove particles or residues on the substrate. It was observed that etching occurs faster near the grain boundary and results in grooved profile. This helps to observe grain boundary better on SEM.

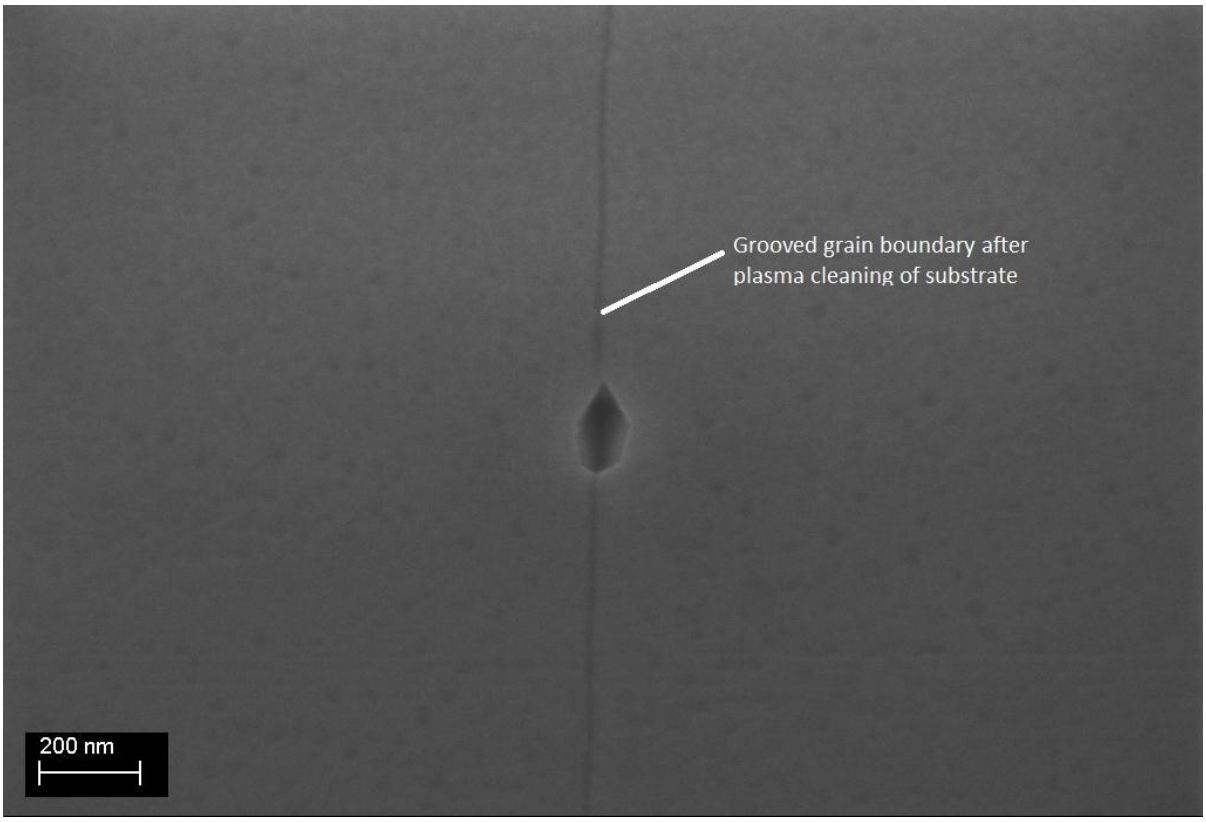

Figure 5.3: Grain Boundary of STO after Ar plasma etching

YBCO Deposition

RF Magnetron Sputtering is extensively used for deposition of YBCO thin films with good quality and superconducting properties. There are several types of geometry used in Sputtering Systems. Off axis and inverted cylindrical magnetron sputtering systems are most promised types among them.[1,26] Generally deposition is done in relatively high pressure of Argon and Oxygen but Low pressure deposition is also reported.[27]. Substrate heating is essential in in-situ deposition of YBCO single crystal thin films and post annealing of thin films for crystallization was also reported.[1,28]

Configuration of our sputtering system was on-axis and substrate target distance was around 15 centimeter. It was equipped with substrate heater capable of heating up to 800 degree Celsius. Argon and Oxygen flows can be controlled into the chamber. And the base pressure of vacuum was $1.2 \times 10^{-5} mbar$. Firstly deposition of in-situ grown single crystal YBCO thin film at 770 C with high ($4 \times 10^{-1} mbar$) and low ($4 \times 10^{-3} mbar$) deposition pressures are tried but it resulted with no significant film deposition on substrate. Room temperature deposition increased the deposition rate more than five times but it was also too low (10 nm per hour) to grow useful thin films in fair amount of time and it requires post annealing of thin films at high temperatures. And it was not possible to test those films because of their thickness was not enough to be observed in EDX.

Then the substrate was placed perpendicular the target at distance of 3 cm and obtain off-axis configuration. It was not possible to heat the substrate in-situ in this configuration. Thin films were deposited at $1.3 \times 10^{-1} mbar$ pressure of Argon Oxygen mixture with %10 oxygen content. Deposition rate was 10 nm/min. Post annealing was used for crystallization of YBCO. Samples annealed at 750 C and atmospheric oxygen pressure showed polycrystalline structure. Then Annealing at low oxygen pressure (29 Pa) was examined .[28] It resulted more uniform thin films with better crystallinity.

SiO_2 Deposition

SiO_2 were deposited using RF magnetron sputtering after post annealing of YBCO. It was done after cool down of substrate to prevent diffusion of Si into YBCO. On-axis configuration was used at $4 \times 10^{-3} mbar$ Argon pressure and 150 W RF Power. Target-Substrate distance was 15 cm and Plasma voltage was 380 V. These conditions were resulted with 40 nm/ hour deposition rate.

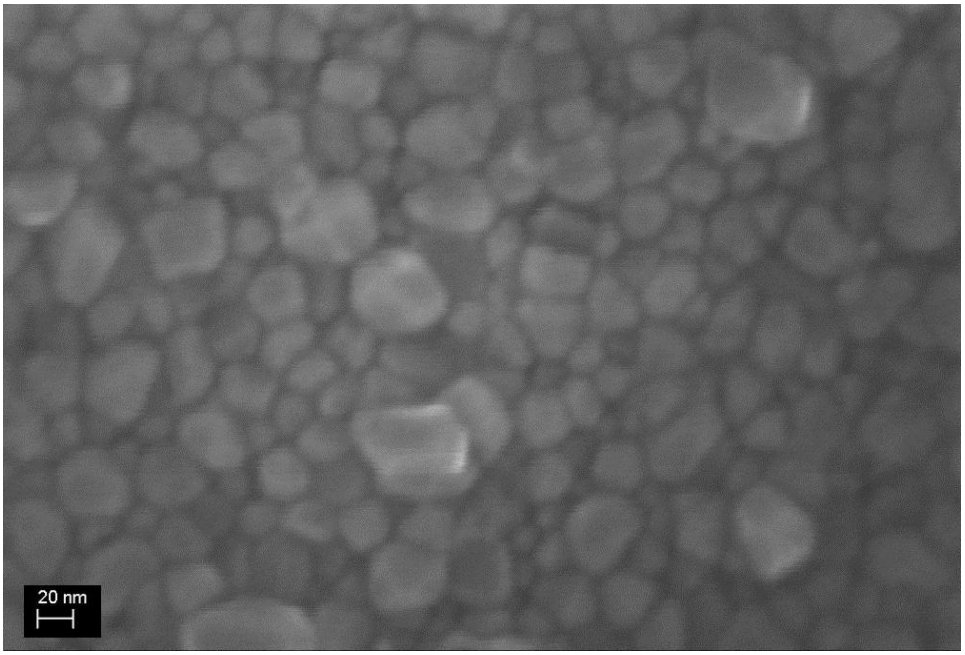

Figure 5.4: YBCO film annealed at 750 C and 300 Torr O_2 atmosphere

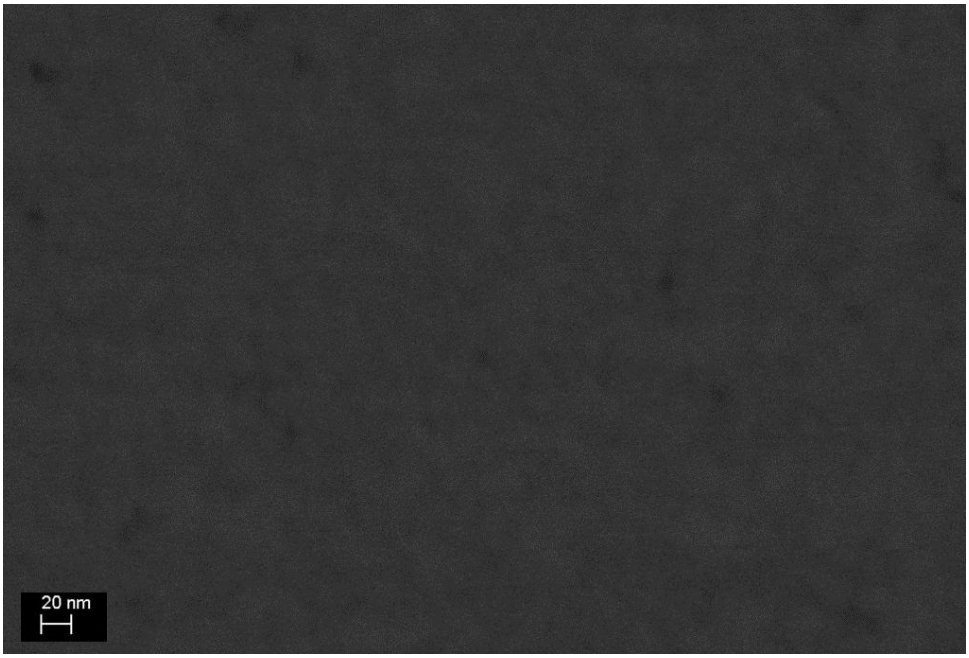

Figure 5.5: YBCO film annealed at 750 C and 29 Pa (220 mTorr) O_2 atmosphere

5.1.2 E-beam Lithography Process

In this process Electron Beam Lithography was used to define patterns on Polystyrene (PS) and these patterns were transferred to SiO_2 by RIE. Molecular weight of PS used was 170 kg/mol. PS was coated as a thin layer onto SiO_2 by spin-coating at 2000 rpm for 40 seconds. Resulted film thickness was 90 nm. 5 kV electron beam voltage was used to expose PS at a dose of 20 $\mu C/cm^2$. PS was developed in Tetrahydrofuran (THF) for 2 minutes. PS is negative resist and unexposed area is etched by developer solution. The grain boundary was visible with the defects along with SEM right before EBL and alignment with grain boundary was possible.

Figure 5.6: Grain Boundary on PS/SiO_2/YBCO/STO sample

5.1.3 Etching

Etching of SiO_2 was performed by RIE with CF_4 and O_2 gases at 20 mTorr pressure with flow ratios 20:2 respectively. RF power applied was 100 W. The etch rate of SiO_2 was 120 nm/min. Patterns on PS were transferred to SiO_2 with this process and SiO_2 was formed as a hard mask for physical dry etching of YBCO.

Physical dry etching of YBCO was realized in the same sputtering chamber applying the RF power to the substrate instead of target. 50 W power and 15 mTorr Argon pressure was used during etching. It resulted with the 1.3 nm/min etch rate of YBCO.[29]

Patterns can barely be seen after etching of YBCO in the SEM pictures below. And the surface of thin film is found too rough after etching. Patterned SQUID loop barely can be seen after etching of YBCO.

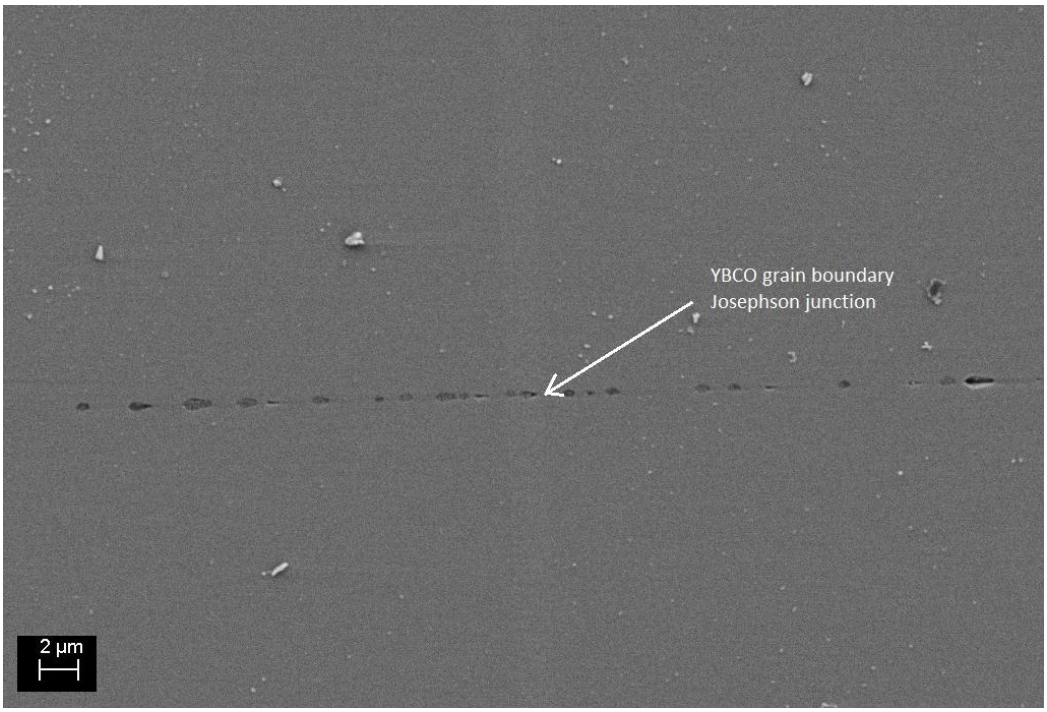

Figure 5.7: YBCO Junction on STO grain boundary

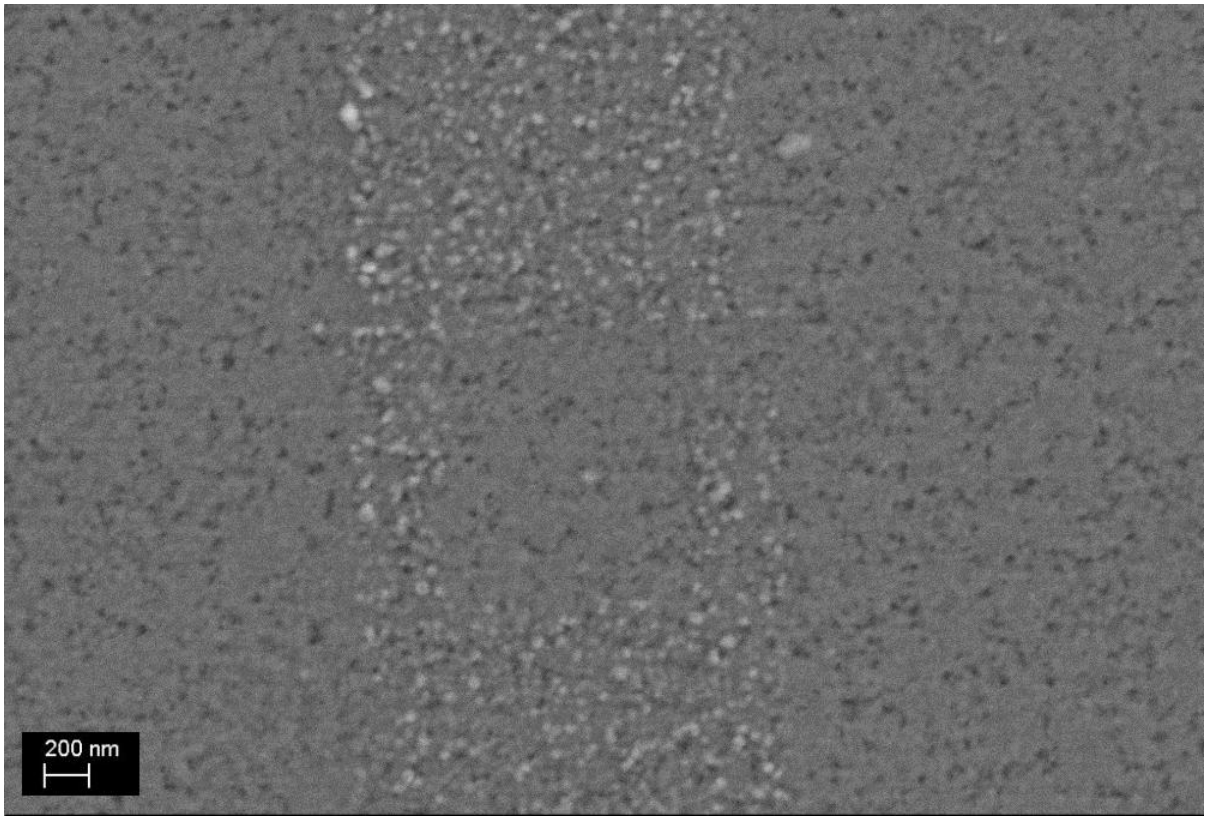

Figure 5.8: YBCO loop formed on STO

5.2 Structural Characterization

Structural characterization of YBCO thin films was done by Scanning Electron Microscopy and Energy Dispersive X-ray Spectroscopy. SEM is a powerful tool to observe surface characteristics of materials in nanoscale. Surface topology and Grain boundary of STO substrates and YBCO thin films were observed with SEM during this study. It was also used for EBL with Nanoscale Pattern Generation System (NPGS) to expose EBL resist PS in desired areas by moving the electron beam. Fabricated patterns on YBCO were also observed with SEM.

EDX was used in this study to observe the composition of YBCO thin films in terms of atomic percentage of elements. The atomic percentages were found in the close vicinity of original stoichiometric ratios of YBCO.

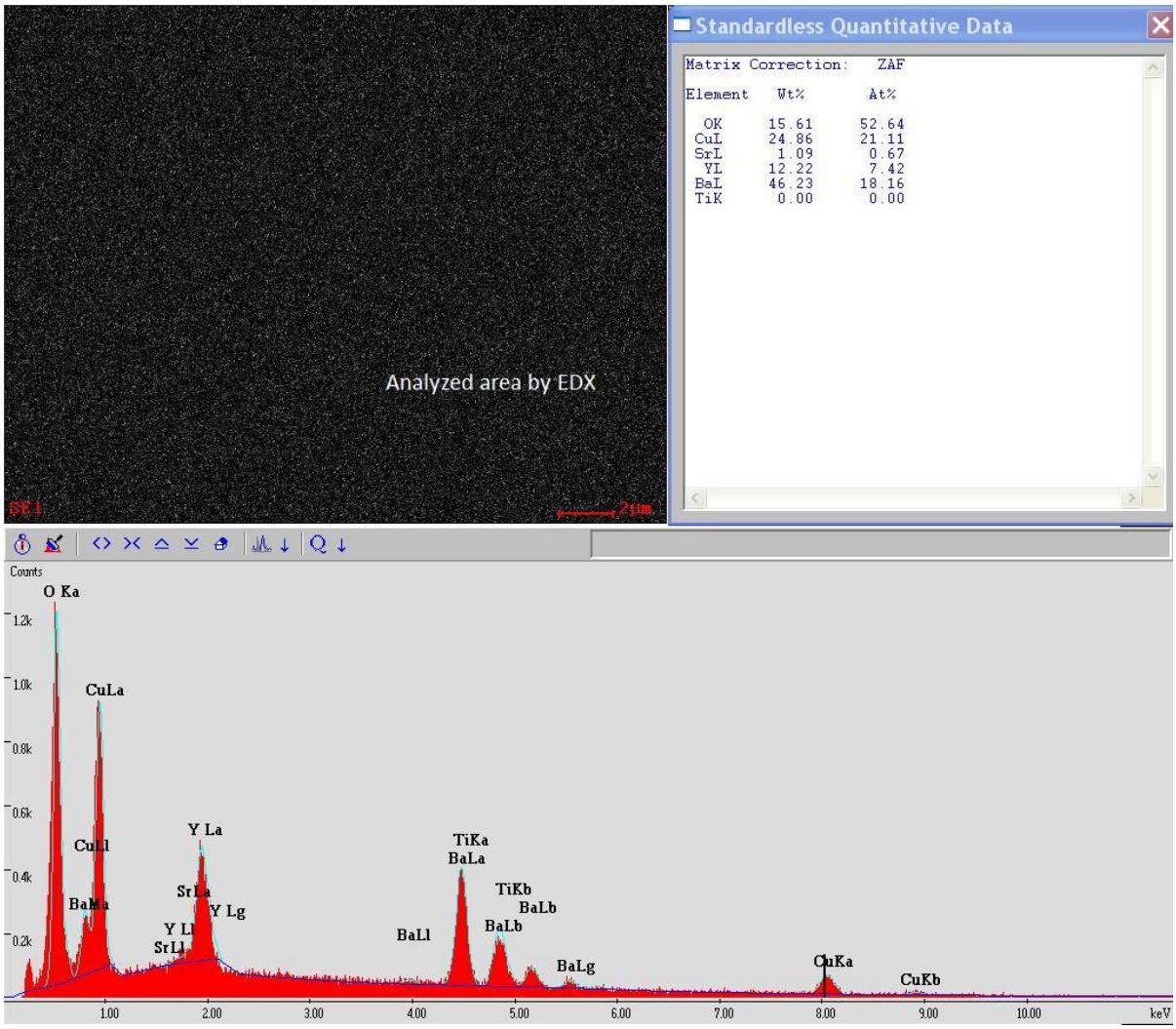

Figure 5.9: EDX results of YBCO thin film

5.3 Electrical Characterization

5.3.1 AC Magnetic Susceptibility Measurements

It was attempted to measure transition temperature of YBCO thin films by observing the diamagnetic transition by magnetic susceptibility measurements. SQUID magnetic property measurement system was used for this purpose at Brockhouse Institute of McMaster University. Magnetic field less than 20 mT which is lower than the lower critical field of YBCO thin film was used to make sure there is no flux penetration into the sample by vortices. Sample was cooled down to 20 K but diamagnetic transition could not be observed. That means samples were not superconducting down to 20 K.

This can be caused by having non-stoichiometric film of YBCO according to Y-Ba-Cu ratios or loss of oxygen content which is necessary to sustain superconductivity on YBCO.

Chapter 6

Conclusion and Recommendations

In this study it was attempted to develop a fabrication process for realization of nanoscale Josephson junctions and SQUIDs. YBCO thin films were deposited by using RF Magnetron Sputtering. SiO_2 was used as an etch mask for physical dry etching of YBCO in Argon Plasma generated by RF source. SiO_2 was patterned by using PS as a negative resist on EBL and transferring the pattern to SiO_2 by RIE. The process was found to be useful for patterning of YBCO thin films but further optimization of process parameters is required to get higher resolution.

Alignment of SQUID loop with grain boundary could not be realized due to lack of control of movement of SEM stage. After locating grain boundary it was not possiblee to follow it because of little angle between x axis of SEM stage and grain boundary direction while it is moving to writing field. Better alignment of grain boundary with x or y axis of SEM stage can solve this problem and alignment of SQUID loop with grain boundary can be realized for nanoscale dimension.

The aim was to fabricate fully functional nanoSQUID and to do magnetic characterization of it but it could not be realized it since deposition of superconducting YBCO thin films was not succesfull. But the developed process for patterning of YBCO and alignment of SQUID loop with grain boundary seems promising for fabrication of nanoscale josephson Junctions and SQUIDs.

It is possible to realize the fabrication of fully functional nanoSQUID with further investigation of developed process. Most important problem was having non-superconducting YBCO thin films with RF magnetron sputtering. In order to overcome this problem, further optimization of deposition parameters needs to be done carefully. Firstly target-subrate distance must be in range of 3 to 5 cm. It is important to get fair deposition rates and to sustain stoichiometric ratio of elements in YBCO.

Oxygen content of thin film is another important parameter for superconducting properties of YBCO. In situ heating of substrate is also required to have better crystallinity of thin film and to increase oxygen richness. Pulsed Laser deposition is another method to obtain high quality YBCO thin films and it can be used to get necessary thin films in this work.

Once superconducting thin films are fabricated it is necessary to optimize the process for patterning these thin films. Resolution of e-beam lithography must be improved to get better defined nanostructures. It can be done by optimizing the exposure parameters for special resist used. Etching process also should be optimized to increase resolution. Surface of thin film was found too rough after sputter etching. In order to have better etching uniformity and etching profile reactive ion etching can be utilized. Etching of YBCO is possible with chlorine based RIE systems.

Electrical and magnetic characterization of fabricated nanoscale Josephson Junctions and SQUIDs needs to be done to finalize this work. Critical current and magnetic response of Josephson Junctions should be observed to confirm the success of the fabrication procedure. Flux quantization should be observed with nanoSQUID as confirmation of their functionality. Measurement of flux sensitivity of fabricated devices should be performed to confirm the demonstrated spin sensitivity of nanoSQUIDs.[3] This can be done by coupling nanoSQUID with magnetic molecules and trying to measure the magnetic flux radiated from these particles.

References

[1] Koelle et al, High-Transition-Temperature Superconducting QUantum Interference Devices, Rev. Mod. Phys. 71, 631, (1999).

[2] Haage et al, Transport properties and flux pinning by self-organization in YBCO films on vicinal STO, Physical Review B, 56(13):8404-8414, (1997)

[3] Nagel et al, Resistively shunted YBa2Cu3O7 grain boundary junctions and low-noise SQUIDs patterned by a focused ion beam down to 80 nm linewidth, Supercond. Sci. Technol., 24 015015, (2011)

[4] Heath et al, Long, Highly-Ordered High-Temperature Superconductor Nanowire Arrays, Nano Lett., 8 (11) 3845–3849, (2008)

[5] Benjamin John Frederick Muller, The Development of a SQUID-based Gradiometer, Thesis MS, Stellenbosch University, (2010)

[6] V. L. Ginzburg and E. A. Andryushin., Superconductivity, World Scientific, (1994)

[7] F. London and H. London., The electromagnetic equations of the supraconductor, Proceedings of the Royal Society of London, A149:71–88, (1935)

[8] J. G. Bednorz and K. A. Müller, Possible high Tc superconductivity in the Ba-La-Cu-O system, Zeitschrift für Physik B Condensed Matter, 64:189–193, (1986)

[9] V. V. Schmidt., The Physics of Superconductors, Springer, (1997)

[10] Orlando,T.P and Delin,K.A , Foundations of Applied Superconductivity, Addison-Wesley, (1991)

[11] Michael Tinkham, Introduction to superconductivity, Courier Dover Publications, (2004)

[12] Harold Weinstock, SQUID sensors: fundamentals, fabrication, and applications, Springer, (1996)

[13] J. Bland, A Mossbauer spectroscopy and magnetometry study of magnetic multilayers and

oxides, Thesis M. Phys, University of Liverpool, (2002)

[14] J. Clarke, A.I. Braginski, The SQUID Handbook: Fundamentals and technology of SQUIDS and SQUID systems, Wiley-VCH, (2004)

[15] J. Clarke, A.I. Braginski, The SQUID Handbook: Applications of SQUIDS and SQUID Systems, Wiley-VCH, (2006)

[16] A.W. Kleinsasser, K.A. Delin, High-TC SNS Josephson Junctions: Moving Beyond Adolescence?, IEEE Transactions on Applied Superconductivity, 7 2: 2964 – 2967, (1997)

[17] R. Gross, L. Al, A. Beck, 0. M. Froehlicht, D. Koelle, A. Marx, Physics and Technology of High Temperature Superconducting Josephson Junctions, IEEE Transactions on Applied Superconductivity, 7 2: 2929 – 2935, (1997)

[18] C. H. Neumann, K. Yamaguchi, K. Hayashi, K. Suzuki, Y. Enomoto and S. Tanaka, Fabrication of high Ic x R, YBCO Josephson- junctions on MgO substrates using a focused ion beam system, Physica C 20, (1993),

[19] J. Hollkott, S. Hu, C. Becker, J. Auge, B. Spangenberg, H. Kurz, Combined method of electron-beam lithography and ion implantation techniques for the fabrication of hightemperature superconductor Josephson junctions, J. Vac. Sci. Technol., B 14: 4100, (1996)

[20] S. E. Babcock, D. C. Larbalestiert, Bicrystal studies of high transition temperature superconductors, Journal of Physics and Chemistry of Solids, 55 10: 1125-1136, (1994)

[21] WFvan Staden, U B¨uttner, V V Srinivasu, WJ Perold, A novel buffered high-Tc superconducting step-edge Josephson junction, Supercond. Sci. Technol., 20: S419–S42, (2007)

[22] A.I. Braginski, High temperature Josephson devices, Physica C: Superconductivity, 185-189, Part 1: 391-400, (1991)

[23] W. H. Mallison, S. J. Berkowitz, A. S. Hirahara, M. J. Neal, K. Char, A multilayer YBa2Cu3Ox Josephson junction process for digital circuit applications, Applied Physics Letters, 68 26: 3808 – 3810, (1996)

[24] B. Ghyselen, M.A. Bari, E.J. Tarte, M.G. Blamire, R.E. Somekh, Y.Yan, J.E. Evetts, Josephson junctions based on c-axis oriented YbaCuO/PrBaCuO/YBaCuO trilayers, Physica C: Superconductivity, 230 3-4: 327-339, (1994)

[25] P.A. Rosenthal, J.E. Cosgrove, D.B. Fenner, L.R. Vale, R.H. Ono, D.A. Rudman, High temperature superconducting step-edge SNS Josephson junctions on silicon substrates, ATER RES SOC SYMP PROC., Vol. 401: 297-302, (1996)

[26] B.P. Algul, Fabrication and Characterization of Superconductor YBCO Josephson Junctions, Thesis MS, İzmir Institute of Technology, (2008)

[27] Sujeet Chaudhary, Subhash C. Kashyap, D. K. Pandya and V. N. Kulkarni, Atomic disorder in low pressure rf-sputtered YBCO superconducting thin films, Physica C: Superconductivity, 280 1-2: 37-42, (1997)

[28] A. Mogro-Campero and L.G. Turner, High quality thin films of YBa2Cu3O7 by post-annealing at low oxygen partial pressure, Physica C, 176 4-6: 429-432, (1991)

[29] S. Knappe, D. Drung, T. Schurig, H. Koch, M. Klinger and J. Hinken, A planar YBa2Cu3O7 gradiometer at 77 K, Cryogenics, 32 10: 881-884, (1992)